ISSN 2436-1550
Online ISSN 2436-2034

Okhotsk Sea and Polar Oceans Research

Volume 7 (2023)

Okhotsk Sea and Polar Oceans Research Association

Mombetsu City, Hokkaido, Japan

Vol. 7

General Information for OSPOR

for OSPOR Vol. 7 (2023)
(July 2022)

1. Aims and Scope

Okhotsk Sea and Polar Oceans Research (OSPOR) is published by the Okhotsk Sea and Polar Oceans Research Association (OSPORA).

Since 1986 the Okhotsk Sea and Cold Ocean Research Association (OSCORA) has held the International Symposium at Mombetsu, Hokkaido, in Japan every February and has released its proceedings over 35 years. In 2017 OSCORA changed to OSPORA, because the Symposium scope was broadened to include the polar oceans (the Arctic and Antarctic Oceans), the Arctic passages, global warming, and environmental change in Polar Regions.

OSPORA started a reviewed papers system from the 2017 Symposium. The papers are refereed by multiple reviewers, published in the proceedings of the Symposium with a title of 'Article' or 'Review', and opened on the OSPOR website.

2. Subjects covered by OSPOR

1) Environment of Okhotsk Sea
2) Meteorology and oceanography in polar regions
3) Cold region engineering
4) Arctic sea routes
5) Global warming and environment change
6) Remote sensing
7) Snow, ice and human life
8) Other topics about Okhotsk Sea and Polar Oceans

3. Editorial Policy of OSPOR

We intend to publish three types of papers;

1) **Article**, containing original scientific materials and results, not submitted for publication elsewhere,
2) **Review**, containing an overview of previous activities, projects and workshops with an outlook of a specific category.

Each of them will be peer-reviewed.

4. Editorial Board

5. OSPOR website

Website: http://okhotsk-mombetsu.jp/okhsympo/top-index.html
E-mail: momsys@okhotsk-mombetsu.jp

Okhotsk Sea and Polar Oceans Research
Volume 7 (2023)

Contents

Okhotsk Sea and Polar Oceans Research 7 (2023) 1-6

https://doi.org/10.57287/ospor.7.1

Review

William Robert Broughton's Voyage of Discovery to the North Pacific and Expedition of the Strait of Tartary / Mamiya Strait

Gaston R. DEMARÉE[1], Yoshio TAGAMI[2] and Patrick BEILLEVAIRE[3]

[1]*Royal Meteorological Institute of Belgium, Brussels, Belgium*
[2]*Faculty of Human Development, University of Toyama, Toyama, Japan*
[3]*French National Center for Scientific Research, UMR CCJ-EHESS, Paris, France*

(Received September October 27, 2022; Revised manuscript accepted December 5, 2022)

Abstract

In the years 1795-1798, the British sloop *Discovery* made a voyage of exploration to the North-West Pacific, the Kurile Islands, the Strait of Tartary / Mamiya Strait and the Japanese, Korean and Chinese coastal areas. The underlying motives of the voyage were geographical survey, putting up settlements, claiming territories, and the long-wished opening of trade with Japan. Nautical and meteorological observations during the voyage are provided on a daily time scale. The sailing through the Strait of Tartary deals with the question of the insularity of Sakhalin / Karafuto which was questioned already by La Pérouse. For this review paper the authors have been mainly guided by Andrew David's annotated version of *William Robert Broughton's Voyage of Discovery to the North Pacific 1795-1798* (David, 2010).

Key words: William Robert Broughton, *Discovery*, Strait of Tartary, Mamiya Strait, meteorology

1. William Robert Broughton

1.1 His personal life

William Robert Broughton was born on 22 March 1762 as the son of Charles Broughton, a gentleman of Hammersmith in the county of Middlesex, and of Anne Elisabeth de Hertoghe. Broughton married his cousin, Jemima Broughton, on 26 November 1802. They had three daughters and one son, William, born on 23 October 1804 at Doddington Hall, Cheshire, who also had a distinguished career in the Navy (Marshall, 1835). On 12 March 1821, having retired to Florence, Captain William Robert Broughton had an angina attack and died two days later. He was buried in the English burial ground in Leghorn (Livorno), Italy (Anonymous, 1821).

Fig. 1 Portrait of William Robert Broughton by an unidentified artist.

1.2 His naval career

William Robert Broughton started his naval career as a Captain's Servant on the *Katherine* in May 1774, then being a midshipman on the *Falcon*, the *Harlem*, the *Eagle* successively, and a master's mate on the *Superb* from December 1778 to January 1782. He became a Lieutenant in January 1782 on the *Burford*. When the *Burford* was paid off in July 1784, Broughton did not serve for almost 4 years. He resumed as a Lieutenant on the *Orestes* and served in the British Channel and in the Mediterranean (June 1788-May 1790), moving to HMS *Victory* in May 1790.

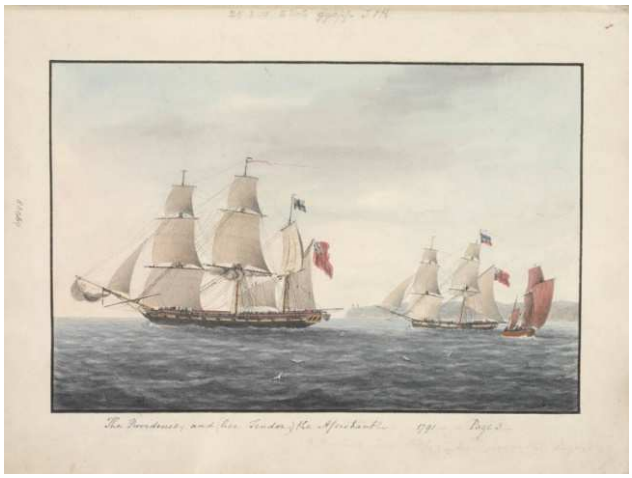

Fig. 2 The H.M.S. *Providence* and (her Tender) the *Assistance* by George Tobin, c. 1791. Mitchell Library, State Library of New South Wales.

Broughton was given command of the brig *Chatham* in December 1790 and was asked to accompany George Vancouver in his exploration of the North-West Pacific. After his arrival in North America in 1792, Broughton charted a group of islands in the Queen Charlotte Sound and explored the lower stretches of the Columbia River in the present-day States of Oregon and Washington. Vancouver sent Broughton back to England via Mexico and the Atlantic, bearing dispatches and requesting instructions (Vancouver, 1797; Lamb, 1984).

Broughton was appointed in command of the *Providence* on 3 October 1793 which took him in a '*Voyage to remote Parts*' (Broughton, 1804). Later on, he served as captain and commanding officer on various ships in the Napoleonic Wars (1803-1815). He became Appointed Companion of the Order of the Bath on 4 June 1815 and Appointed Colonel of Marines on 12 August 1819.

2. William Robert Broughton's Voyage

2.1 The Voyage of the Providence from England to Macau

The *Providence*, a Royal Navy sloop, mounting 12 guns, weighing about 406 tons, purchased from the stocks at Blackwell Yard from John Perry on 23 April 1791, was high suitable for distant voyaging (see Three Decks, *Providence*). On 2 October 1794, she was put under the command of William Robert Broughton who states: 'I received my orders, which were secret'. Following his narrative, on 15 February 1795 'The whole fleet was under way' under a favorable north wind. On Thursday 5 March 1795, 'Early in the morning, saw the Canary Islands', and on 5 May, 'the weather prevented our reaching the entrance of Rio Janeiro harbor'. The *Providence* then crossed the South Atlantic Ocean and the Indian Ocean and 'moored in Sydney Cove' in Australia on 18 August. On 29 November 1795, she anchored at Matavai Bay [Tahiti], reached Owhyhee [Hawai'i] in January 1796, and anchored on 15 March 1796 'In the Entrance of Nootka Sound [on the west coast of Vancouver Island, in the Pacific Northwest], under Light Breezes and Cloudy **we**ather with slight Showers of Hail. The whole Country was cover'd with Snow presenting a most dreary Aspect.'

As 'several Letters dated in March 1795 inform'd [Broughton] of Captain Vancouver having sail'd for England', he made his way south and entered Monterey Bay, Mexico, on 6 June 1796, where he received a cold reception. He therefore decided to survey the coast of Asia from Sakhalin to the Yangtze River in the hope of opening trade with Japan (King, 1997, 2010). On 20 June he departed from Monterey [Mexico], bound for Hawai'i in order to rate his chronometers. On 31 July, he left Hawai'i. 'At daylight on 7 September we descry'd the Land of Japan', Broughton writes. 'Sailing to the north near Port Nambu [Miyako-wan]', he then reached Uchiura-wan, named by him Volcano Bay, on Ezo [Hokkaidō]. He anchored in Endermo [Muroran-kō] where he found the Ainu and the Japanese friendly and helpful.

Broughton left Endermo on 1 October sailing to the north towards the Kurile Islands. These islands had already been explored by Europeans like Maarten Gerritszoon de Vries on the *Castricum* in 1643 (Leupe, 1858), Spanberg on the *Arkhangel Mikael* in 1739 (Muller, 1766), and in the aftermath of Cook's third voyage (1776-1779). On 5 October, Broughton notes: 'At Sunset, we passed two Islands near the Main [Habomai islands]' and on the 7th [we] went NNW through the Passage of the Kunashiro-suidō [Yekateriny Strait] separating Kunashiri-tō and Etorofu-tō. On 16 October, Broughton reached the Island of Marukan [Ostrov Simushir] where 'The settlement of the Russians', known from Cook's third voyage, was 'found abandoned; but they cou'd not learn from the Natives at what period. … I did not propose this Year to go further to the North owing to the advanced State of the Season.'

Broughton hence set course to the southwest and successively reached the southeastern extremity of Honshū and the islands of Edo-wan on 10 November, Okinawa on 1 December, and the east coast of Taiwan on 6 December. He eventually dropped anchor on 12 December 1796 in Macao 'having been two Years from England without any communication.' (Broughton, 1804; Hoare, 2000; David, 2010).

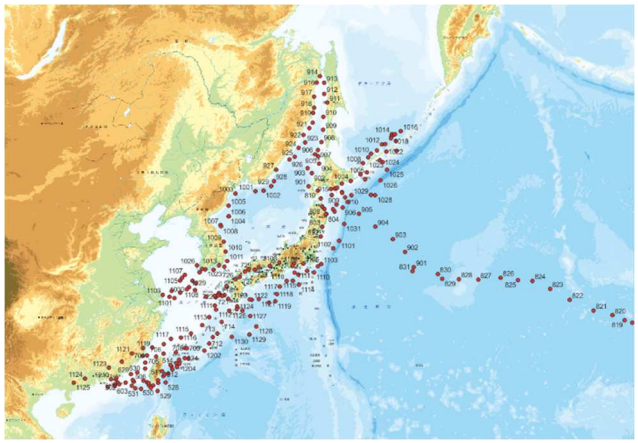

Fig. 3 Voyage of the *Providence* across the Pacific Ocean, to Japan, the Kurile Islands, Macau and again the Ryūkyū Islands with the wreckage of the *Providence*, and the continuation on the schooner to Japan, the Strait of Tartary / Mamiya Strait and return along the coast of Siberia, Korea and China to Macau and thence to England.

2.2 Second expedition to the North and return to England

Broughton 'hearing there was a Small Vessel for sale' bought, on 29 December 1796, the 87-ton registered

schooner *Prince William Henry* 'as an Assistant in surveying' but mainly to reduce the risk of navigating with a single vessel in uncharted waters. On 11 April 1797, they 'got under weigh' voyaging again to the north. By the end of April, 'our People being afflicted with a Dysentery which we cou'd only attribute to the Hazey and Foggy weather', meteorological conditions being thought to be responsible in the context of the integrated 18th century Hippocratic hypothesis on medicine, climate and environment. 'We lost the whole of our Pigs … they were equally with ourselves troubled with the Dysentery.' (Demarée, 1996)

In the evening of 17 May 1797, the *Providence* 'Struck upon a Reef of Coral Rocks' north of Ikema-jima, near Miyako-jima. She was completely wrecked, but the full crew could be conveyed to the schooner. However almost all of the equipment was lost. The schooner anchored at Miyako-jima where the inhabitants were very helpful. After being well supplied, Broughton decided to sail the schooner back to Macau. As he planned to continue the survey to the north on the schooner with a limited crew, he made the necessary arrangements for the transfer of the discharged personnel to England. On 15 June, 'we sail'd a second time in the prosecution of the voyage' with 'a prospect of acquiring geographical knowledge of the Tartarean & Corean coasts'.

Broughton sighted the Pescadores Islands, west of Formosa [Taiwan], on 30 June, and, rounding the northernmost point of Taiwan, reached Okinawa-guntō on 8 July. He dropped anchor at Naha-kō, Okinawa, on 10 July, where provisions and water were readily sent off to the schooner. 'Our Friends did not seem to wish we shou'd go onshore', he notices then. Setting course north and passing along the east coast of Honshū, he reached once again Muroran-kō, Hokkaidō, on 12 August, where '[the crew] immediately commenced [the] necessary operations of refitting the Vessel & preparing for Sea.' The schooner raised the anchor on 23 August, approached Hakodate-wan on the 30th and Matsumae, on the west coast of Hokkaidō, the next day: 'The town was ascending gradually up the Rising grounds Interspers'd with Trees & Gardens. … The superior Houses were decorated by long pieces of color'd Cloths …'. Broughton, who frequently refers to La Pérouse's voyage in July 1787, was able to go eight miles farther than him in the Strait of Tartary. He then sailed southwards along the Asian continent. After sighting the island of Tsushima (situated between South Korea and Japan) and calling in Busan Harbor for a week, he steered the schooner through the Korean archipelago and along the Chinese coast, finally reaching Macau on 27 November 1797. (Broughton, 1804; Hoare, 2000, David, 2010)

3. Nautical, astronomical and meteorological Observations

The book published by W.R. Broughton in 1804 contains as Appendix No. I the 'TABLES of the ROUTE of the PROVIDENCE and her Tender, the Variation of the Compass, and the State of the Barometer and Thermometer, during the Voyage from the Sandwich Islands, July 31st 1796, till our last Arrival at Macau, November 27th 1797.' Fragments of these meteorological observations are given in Kubota *et al.* (2018a, 2018b). However, the nautical and astronomical observations mentioned as Latitude observ'd or indifferent, Latitude account, Longitude *ditto* and Longitude within the annotated version of Broughton's Voyage are used in this paper (David, 2010).

It is known that barometers and thermometers were on board of the *Providence* as the Navy Board instructed to supply Broughton in 1794 with instruments. It is further supposed 'to note the height of one or more Thermometers placed in the Air, and in the Shade early in the Morning and about the hottest time of the day, and to observe also the height of the Thermometer within the Vessel near the Watches'. Unfortunately, no further information on the thermometric and the atmospheric pressure observations is given. In particular, the double set of thermometric observations remains a problem. A thermometer disappeared when 'the Ship was lost', that is, when the *Providence* wrecked on a coral reef.

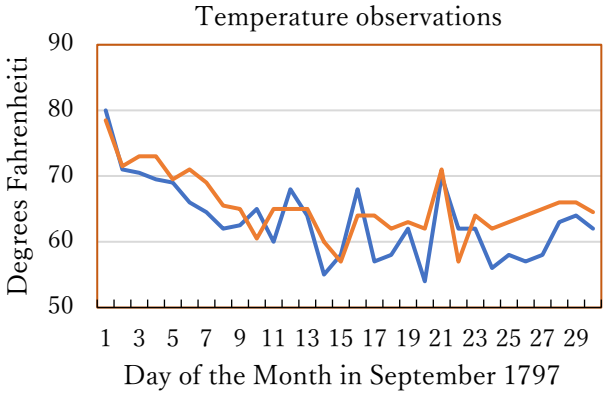

Fig. 4 Graph of both unspecified sets of temperature observations in the Strait of Tartary / Mamiya Strait in September 1797.

A graph of both sets of daily temperature observations carried out when sailing through the Strait of Tartary in September 1797 is shown in Fig. 4. In these days, the schooner sailed on through Tsugaru-kaikyō on 30 August and viewed the town of Matsumae, Hokkaidō, on the next day, while on 15 September the latitude of 51° 45' 7'' N was reached. The temperature difference equals 13,055°C for a difference of 10,108-degree latitude providing a decrease of 1,29°C per unit degree latitude.

4. The question of the insularity of Sakhalin

The insularity of Sakhalin / Karafuto remained an unsolved question until the mid-19th century. Jean François de La Pérouse, William Robert Broughton and Adam Johann von Krusenstern had already sailed into the Strait of Tartary, but without traversing it (Boyle, 2018). La Pérouse and Broughton approached the Strait from the south while Krusenstern approached it from the Sea of Okhotsk. The question was solved by the Japanese explorer Rinzō Mamiya (1775-1844) in 1808-1809 (see Figure 5) who confirmed the insularity of Sakhalin (Stone, 1996; McVey, 2022). The information was kept secret by the Japanese and later on by the Russians but Philip Franz von Siebold (1796-1866) mentioned the name of Mamiya Strait and published a map in his book "*Nippon*" in The Netherlands, although the deliveries of any topographical and hydrological data to foreign countries had been prohibited by the Shogunate (Siebold, von, 1832-). That knowledge proved to be primordial to the Russians in the Far-Eastern developments of the Crimean War (1853-1856). After the defeat of the British and French fleets at Petropavlovsk, Kamchatka, in August-September 1854, the allies thought to have trapped the Russians in the Strait of Tartary in May 1855: 'However, the Russians passed through the Strait and entered the Amur River, much to the deep embarrassment of the British and the fury of the press' (Stephan, 1969; Beillevaire *et al.*, 2018).

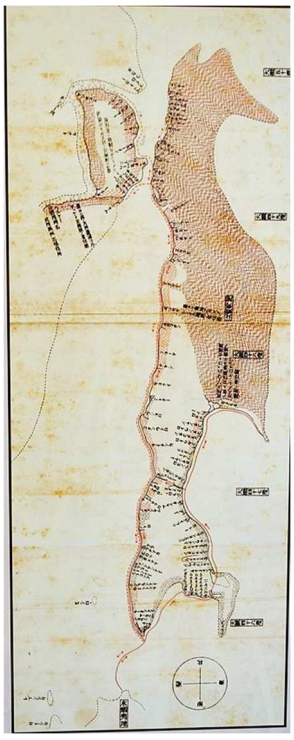

Fig. 5 Map of Sakhalin and Lower Amur, compiled by Rinzō Mamiya in 1808-1809 (Mamiya Rinzō, courtesy of Wikipedia).

On 9 July 1787, the latitude of La Pérouse's vessel in the Strait of Tartary was 48° 15' N. On 12 July, La Pérouse and Langle accompanied by several others landed on Sakhalin and met a group of native people. The offering of presents led to friendly interactions: 'We contrived at length to make them understand that we wished them to delineate their country, and that of the Manchous. One of the old men then rose, and with his pike traced the coast of Tartary to the west, running nearly north to south. Opposite this, to the east, he drew his own island, in the same direction, laying his hand upon his breast, to indicate that he just traced his own native country. Between the island and Tartary, he left a strait; and turning to our vessels, which lay in sight, he signified by a stroke, that they may pass through it.' La Pérouse learned also from the natives 'the breath and the depth of the strait that separated his own country from Tartary'. (La Pérouse, 1807)

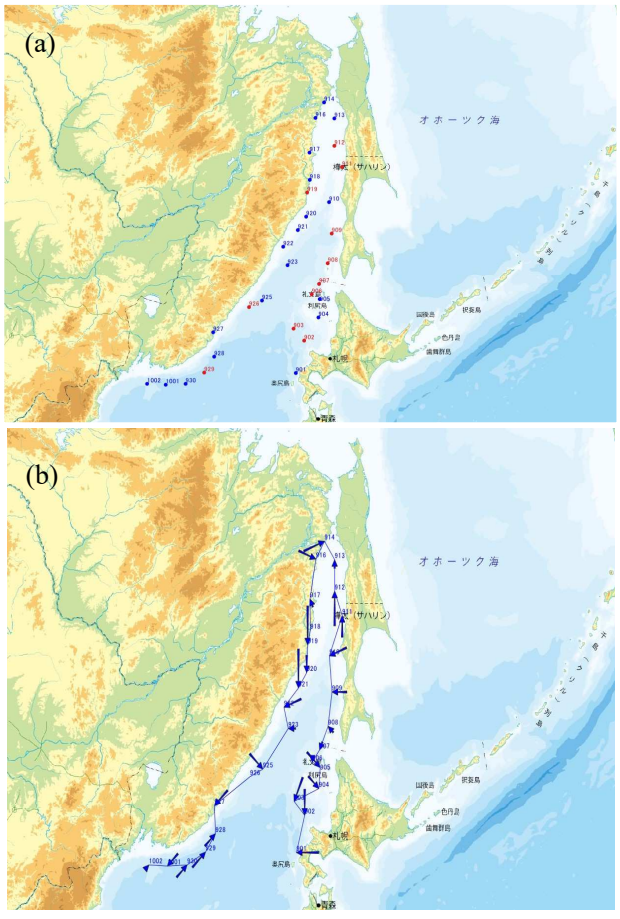

Fig. 6a & 6b. Travel of the schooner in July 1797 in the Strait of Tartary / Mamiya Strait. The dots indicate the location of the vessel. The accounted latitude and the accounted longitude are shown in red dots while the accounted latitude and longitude by watch are shown in blue dots. Also, winds are shown by the wind force in the afternoon and wind direction in the afternoon.

On 20 July 1787, 'Being obliged to keep one coast or the other, I had preferred that of the island, to ensure not missing the strait, if one existed to the east; which required extreme attention, on account of the fogs, which left us very short intervals of clear weather. … The channel begins to narrow in the parallel of 50°, and had not thenceforward above twelve or thirteen leagues in breadth.' On the 23 July 1787, the latitude observation gave 50° 54' N and La Pérouse thought he 'was too far advanced not to wish to reconnoitre this strait, and to know whether it was passable; though [he] began to fear it was not, as the depth of the water diminished very fast as [they] proceeded north, and the land of Sagaleen island [Sakhalin] consisted no longer of anything but downs, inundated with water, and almost level with the sea, like sand-banks.' At the end of July 1787, La Pérouse 'having found the impossibility of getting out of this channel to the north', and taking into account navigational and meteorological difficulties, decided instead to follow the coast of Tartary southwards. (Broughton, 1807).

On Thursday 14 September 1797, on the schooner, Broughton writes: 'In crossing over and as we approach'd the west Shore, our soundings decreas'd to 9 *fatho*ms. No Land from N. 15° E. to N. 53° E., but from thence a continuation of very low Hummocks just appearing above the Horizon. The Master [William Chapman] was sent to make further Remarks to the North.' On Friday 15 September, 'At Dark, the Master return'd who reported having found round the nearest point, which bore N 10° E from us, a Bay [Bukhta Sushcheva] leading to the Westward … The Master gave it as his Opinion the passage through seemd pretty evident. The observ'd latitude made 51° 45' 7'' N'. On Saturday 16 September, 'from the Masthead we plainly discern'd very low Land extending over the NE of the Bay. … and we were fully satisfied there was no opening to the Sea in the direction the Master suppos'd.' (Broughton, 2010, p. 172-173) However, a hesitating Broughton's took the following decision: 'as the Master had represented the bay unfavourable, even supposing we could get there, which I deemed from the shallow water leading to it impracticable, without great risk of the vessel… induced to me to lose no more time, as the equinoxes were approaching, to proceed to the southward.' (Broughton, 1804, p. 302)

Adam Johann von Krusenstern did interpret that La Pérouse 'very rightly concluded that either Sachalin was connected with Tartary, or that the channel which separates the two countries must be very narrow, and at upmost only a few feet in depth. … Our observations, which were carried out one hundred miles more to the north, leave no doubt upon the subject … We already found a considerable difference in the weight of water … and finally when close to the channel that separates Sachalin to the northward of the Amur from Tartary, the water drawn up the ship's side was perfectly sweet. When Krusenstern read Broughton's book on his arrival in China, he found his ideas upon the junction of Sachalin with Tartary well founded and concluded: 'What therefore, since La Pérouse, has been called a channel, must now take a new name, and be known as the gulf of Tartary'. (von Krusenstern, 1813)

Gennady Ivanovich Nevelskoy (1813-1876), in command of the Amur Expedition (1849-1855), explored the Sea of Okhotsk, the outlet of the Amur River area and Sakhalin. He definitely proved the insularity of Sakhalin showing that it is a strait connected to the Amur estuary by a narrow section. The northernmost narrowest section is known as the Strait of Nevelskoy in honor of Captain Nevelskoy (Samochwalow, 1871; Genady Nevelskoy, Wikipedia).

5. Conclusion

William Robert Broughton's voyage of *Discovery* to the north-east Pacific and to the coastal areas of Japan, Korea, China, the Ryūkyū Islands, the Kurile Islands, Sakhalin and the Strait of Tartary / Mamiya Strait has been a significant contribution to the geographical knowledge of these areas. He follows earlier Dutch, French, Russian and other British navigators in exploring the geography of the Asian continent and the location of numerous islands in that part of the world. The tentative interactions of Broughton with Japan and its inhabitants might be seen in the context of the long-wished desire of opening trade with the Shogun Ruled Japan. At the same time, Broughton expressed his view in the long-lasting question of the insularity of Sakhalin believing, in contrast to his Master, that there was no opening. Rinzō Mamiya discovered the narrow navigable channel in 1808-1809, rediscovered by Nevelskoy in 1849, but that strategical intelligence was kept secret by Japan and the Russia.

Acknowledgements

The authors sincerely acknowledge the constructive remarks and suggestions by two anonymous reviewers.

References

Anonymous (1821): *Capt.* William Robert Broughton – *Obituary*. *The Gentleman's Magazine: and Historical Chronicle.* From January to June, 1821. Volume XCI. (Being the Fourteenth of a New Series.) Part the First, 376-377.

Beillevaire, P., G.R. Demarée and T. Mikami (2018) : La campagne en Asie orientale de Jean Barthe, chirurgien naval, météorologue et naturaliste (1855-1857). *Bull. Séanc. Acad. R. Sci. Outre-Mer / Meded. Zitt. K. Acad. Overzeese Wet.,* **64** (2018-1), 105-144.

Boyle, E. (2018): Cartographic Exchange and Territorial Creation: Rewriting Northern Japan in the Eighteenth and Nineteenth Centuries. In: M. Altić *et al*. (eds.) *Dissemination of Cartographic Knowledge, Lecture Notes in Geoinformation and Cartography*. International Research Center for Japanese Studies, 75-98.

Broughton, W.R. (1804): *A Voyage of Discovery to the North Pacific Ocean: in which the coast of Asia, from the Lat. of 35° North to the Lat. of 52° North, the Island of Insu (commonly known under the name of the Land of Jesso,) the North, South, and East coasts of Japan, the Lieuchieux and the adjacent Isles, as well as the coast of Corea, have been examined and surveyed. Performed in his Majesty's sloop Providence and her Tender, in the Years 1795, 1796, 1797, 1798*. London, T. Cadell and W. Davies.

David, A. (Editor), Introduction by Gough, B. (2010): *William Robert Broughton's Voyage of Discovery to the North Pacific 1795-1798*. London, The Hakluyt Society, Third Series, 22, LXX, 315 p.

Demarée, G.R. (1996) The neo-hippocratic hypothesis – an integrated 18th century view on medicine, climate and environment. Proceedings of the International Conference on Climate Dynamics and the Global Change Perspective, Cracow, October 17-20, 1995, p. 515-518.

Hoare, J.E. (2000): Captain Broughton, HMS *Providence* (and her tender) and his Voyage to the Pacific Ocean 1794-8. *Asian Studies*, **31**, 3 (October 2000), 303-312.

King, R.J. (1997): A regular and reciprocal System of Commerce – Botany Bay, Nootka Sound, and the Isles of Japan. *The Great Circle*, ***19***(1), 1-29.

King R.J. (2010): "The long wish'd for object" - Opening the Trade to Japan, 1785-1795. *The Northern Mariner / Le marin du nord*, XX, 1-34.

von Krusenstern, Captain A.J. (1813) *Voyage around the World in the Years 1803, 1804, 1805, & 1806 by order of his Imperial Majesty Alexander the First on Board of the ships Nadeshda and Neva …* Vol. I., London, 404 p.

Kubota, H., R. Allan, C. Wilkinson, P. Brohan, K. Wood and M. Mollan (2018a): Recovery of climate around Japan during the late Edo era using meteorological observation data recorded in foreign ship logs sailed to Japan, Meteorological Society of Japan Fall meeting 2018, B366.

Kubota, H., R. Allan, C. Wilkinson, P. Brohan, K. Wood and M. Mollan (2018b): 外国船の航海日誌に記載された気象データから復元する江戸時代後期の日本周辺の気候 - Recovery of Japan climate during late Edo era by foreign ship logs, The Association of Japanese Geographers Spring meeting, C000324.

Lamb, W. Kaye (Ed.) (1984): *George Vancouver, A Voyage of Discovery to the North Pacific Ocean and Round the World*. Hakluyt Society, Second Series, 163-6, 4 volumes, London.

La Pérouse, J.F.G. (1807): *A Voyage round the World performed in the years 1785, 1786, 1787 and 1788 by the Boussole and Astrolabe*. London, Vol. II.

Laughton, J.K. (2004) *Broughton, William Robert, naval officer, (1762-1821)*, rev. Roger Morris. Oxford Dictionary of National Biography, Oxford University Press, online edition, May 2006.

Leupe, P.A. (1858) *Reize van Maarten Gerritsz. Vries in 1643 naar het Noorden en Oosten van Japan, volgens het Journaal gehouden door C.J. Coen, op het schip Castricum. Naar het handschrift uitgegeven en met belangrijke bijlagen vermeerderd door P.A. Leupe, ...* Frederik Muller, Amsterdam. 440 p.

Mamiya Rinzō. https://en.wikipedia.org/wiki/Mamiya_Rinzō

Marshall, J. (1835): *William Broughton, Esq.* Royal Naval Biography; or, memoirs of the Services …, Vol. IV, Part II, London, 474-477.

McVey, K.Y. (2022) Intelligence journey up the Amur: Mamiya Rinzo's observation in 1809. European Association of Japan Resource Specialists (EAJRS), 17 October 2022, Lisbon, https://www.youtube.com/watch?v=94-jkLMqx44.

Nevelskoy https://en.wikipedia.org/wiki/Gennady_Nevelskoy

Samochwalov, S.P. (1871): *Anleitung zur Befahrung der Tatar- oder Sachalin-Strasse, wie des Amur Limans*. Herausgegeben von H.J. Pallisen. Hamburg, L. Friederichsen & Co., 217 p.

Siebold, Ph.Fr. von (1832-) Archief voor de beschrijving van Japan en deszelfs toegevoegde en cynsbare landen : Jezo met de zuidelijke Kurilen, Krafto, Koorai en de Liu-Kiu-eilanden, volgens Japansche en Europische geschriften en eigene waarneming bewerkt door Ph.Fr. von Siebold. ... Leyden, Lith. van het Nippon Archief.

Stephan, J.J. (1969): The Crimean War in the Far East, *Modern Asian Studies*, **3**, 268-274.

Stone, I.R. (1996): W.R. Broughton and the Insularity of Sakhalin. *The Mariner's Mirror*, **82**, 76-81.

Three Decks–Warships in the Age of Sail. *William Robert Broughton (1762-1821) – British Sixth Rate discovery vessel 'Providence'*. https://threedecks.org/index.php?display_type=show_crewman&id=2175 https://threedecks.org/index.php?display_type=show_ship&id=6010

Vancouver, G. (1798): *A Voyage of Discovery to the North Pacific Ocean, … and performed in the Years 1790, 1791, 1792, 1793, 1794, and 1795 in the Discovery Sloop of War, and the Armed Tender Chatham, under the Command of Captain George Vancouver.* In three Volumes. London.

Summary in Japanese

和文要約

W. R. Broughton のタタール海峡/間宮海峡の探検航海

Gaston R. DEMARÉE [1], 田上善夫 [2], Patrick BEILLEVAIRE [3]

[1] ベルギー王立気象研究所, [2] 富山大学, [3] フランス国立科学研究センター

1795 年から 1798 年にかけて、イギリスのスループ船ディスカバリー号は、北西太平洋、千島列島、タタール海峡/間宮海峡、日本、韓国、中国の沿岸地域への探検航海を行った。航海中は毎日規則的に気象観測が行われた。タタール/間宮海峡での航行は、ラ・ペルーズが疑問視していたサハリン/樺太が島かどうかの問題を扱っている。

Correspondence to: G. R. Demarée, gaston.demaree@meteo.be

Okhotsk Sea and Polar Oceans Research 7 (2023) 7-12

https://doi.org/10.57287/ospor.7.7

Review

Full-scale Experiments of JCG Patrol Vessel SOYA from 1991 to 2013 in the Southern Sea of Okhotsk

Takatoshi MATSUZAWA[1], Haruhito SHIMODA[1], Tadanori TAKIMOTO[1], Daisuke WAKO[1]
Koh IZUMIYAMA[2] and Shotaro UTO[2]

[1]*National Maritime Research Institute, National Institute of Maritime, Port and Aviation Technology, Tokyo, Japan*
[2]*Arctic Research Center, Hokkaido University, Sapporo, Japan*

(Received September 30, 2022; Revised manuscript accepted December 30, 2022)

Abstract

The winter navigation in the southern Sea of Okhotsk needs ice-strengthened vessels due to sea ice. In this region, the Japan Coast Guard has operated patrol vessels, such as P/V SOYA, capable of ice navigation and provided valuable opportunities for ice observation and ship ice trial. National Maritime Research Institute took part in such cruises for twenty-three years and conducted full-scale onboard experiments regarding ice conditions and ship performances in ice. This paper overviews the experiments with the measurement results of ice concentration, ice thickness, ice load on the hull, and shaft power required in ice. The long-term data accumulation in response to various ice conditions would contribute to the design and operation of forthcoming Japan Coast Guard patrol vessels.

Key words: ship characteristics in ice, icebreaker design, onboard measurement

1. Introduction

The Sea of Okhotsk is the southern limit, in the Northern Hemisphere, of drift ice usually coming ashore along the coast of Hokkaido between late January and early March. The Japan Coast Guard (JCG) deploys the patrol vessels (P/Vs) SOYA and TESHIO, which can operate in ice-covered waters with ice-breaking ability to deal with maritime accidents in drift ice. National Maritime Research Institute of Japan (NMRI) conducted full-scale experiments in ice onboard P/V SOYA (Fig. 1) and supplementally P/V TESHIO from 1991 to 2013 in the coastal area of Hokkaido, and the most of these experiments were conducted under a joint research agreement with the Ship Division, Equipment and Technology Department of the JCG. The above research series is referred to as the Joint Ship Research or abbreviated to the JSR. In this paper, we discuss the experiments onboard P/V SOYA.

Fig.1 P/V SOYA operating in ice

The purpose of the JSR was to study the sea ice conditions in the southern Sea of Okhotsk, and to clarify ship performance in ice-covered waters, and hull loading caused by contact with ice (hull ice load) through observations based on the actual vessel and to collect practical information to the development of forthcoming P/Vs of JCG operated in ice.

One of the worthiness of the series of experiments is the long-term data accumulation in response to various ice conditions repeatedly obtained by the same vessel. Sea ice in the southern Sea of Okhotsk is first-year ice showing various forms in respective years. Therefore, the data contains ice contact events experienced in various ice conditions and reveals the operation profile of the patrol vessels in ice.

The results of these experiments have been published in various forms and literature. However, there have been few reports that summarize overall experiments. This paper summarizes the results of the JSR obtained onboard P/V SOYA. The comprehensive measurements of ship characteristics in the southern Sea of Okhotsk for decades have been rarely reported yet due to the lack of icebreaking operation experiences by Japanese vessels. These measurements provide a unique dataset for icebreaker design and winter navigation in the Sea of Okhotsk.

2. Outline of the Full-scale Experiments

Figure 2 shows the history of the full-scale experiments conducted by NMRI onboard JCG P/Vs. In

1991, NMRI started full-scale experiments in the ice-covered area along northeastern Hokkaido onboard patrol vessels in collaboration with JCG. P/V SOYA has been the most eligible for the purpose, whereas P/V TESHIO was temporarily engaged several times since its launching in 1995 (Koyama *et al*., 2000.) Since 1996, P/V SOYA and the 1st Regional Coast Guard Headquarters have provided annual scientific cruises in the middle of February along the route planned shown in Figure 3 mainly for sea ice observation mission in cooperation with Institute for Low Temperature Science (ILTS), Hokkaido University and other academic parties. NMRI had taken these opportunities to carry out a variety of measurements for engineering purposes until 2013.

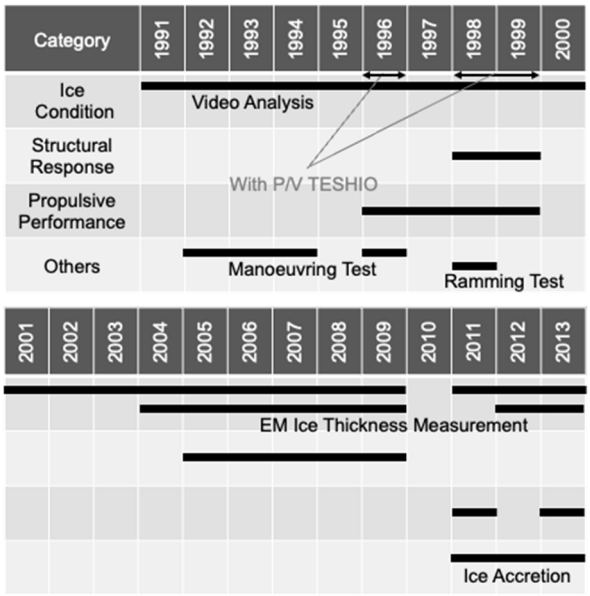

Fig. 2 History of Full-Scale Experiments by NMRI onboard JCG P/Vs

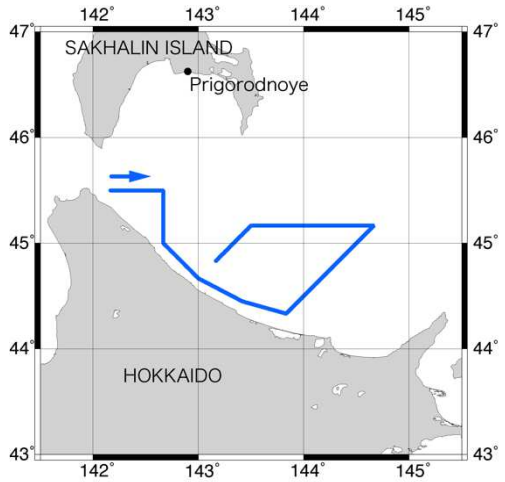

Fig.3 Typical route in the scientific cruises of P/V SOYA in the southern Sea of Okhotsk

P/V SOYA was constructed as the first patrol vessel capable of carrying a helicopter in JCG and entered service in 1978. Table 1 shows the principal dimensions. The hull is ice-strengthened to the level approximately equivalent to IA Super in the Finnish-Swedish Ice Class Rules (FSICR). P/V SOYA has a twin-shaft diesel propulsion system equipped with controllable pitch propellers (CPP), providing power for the ice-breaking ability for level ice of 1.0m thick. In addition, anti-rolling tank and retractable fin stabilizers are equipped to suppress adverse rolling in helicopter operation.

Table 1 Principal Dimensions of P/V SOYA

Item	Unit	Value
Length Overall	(m)	98.6
Length Waterline	(m)	90.0
Breadth Molded	(m)	15.6
Depth Molded	(m)	8.0
Draft	(m)	5.2

The significant parameters obtained onboard icebreakers for engineering purposes are:

a. ice concentration and thickness as environment condition,
b. hull structural response for hull ice load, and
c. shaft thrust and torque for propulsion performance in ice.

The ice concentration and thickness measurements were carried out in collaboration with the onboard scientific observation conducted by ILTS, and the results have been combined in the annual reports (ILTS, 1996-2022.) We also measured the hull structural response, the thrust, and the torque together with the above scientific observation. The results of these measurements are respectively explained later.

3. Ice Conditions in the Sea of Okhotsk off the Hokkaido Coast

From an engineering point of view, ice properties such as ice concentration, thickness, floe size, and mechanical strength are essential parameters for the design and operation of ice-going vessels. In this region, ILTS has continued the long-term visual observation of sea ice features based on ASPeCt protocol initially proposed for Antarctic ice, which reveals that the dominant thickness categories are thin first-year ice (from 0.3 to 0.7m) and nilas (under 0.1m) during recent 20 years, for example. It is also reported that the average thickness is 0.28m for level ice and 0.65m for ridged ice, which indicates that the ridging process is vital for the growth of ice thickness in this area.

NMRI adopted the ship-borne video analysis methods for sea ice concentration and thickness. Figure 4 shows the analysis method of ice concentration. Ice concentration is automatically calculated by pixels on

the fixed horizontal line in each binarized video frame of the front view.

Figure 5 shows how to measure ice thickness from video images. Ice thickness is directly measured from downward-looking views in which a broken ice piece stands the side-up position (Shimoda *et al.*, 1997). Figure 6 shows the histogram of total thickness from 1991 to 1998 (Uto *et al.*, 1999) by the video analysis method. Here total thickness denotes the sum of ice thickness and snow depth. Although this method is accurate for undeformed ice, it is difficult to obtain data of very thin or thick deformed ice.

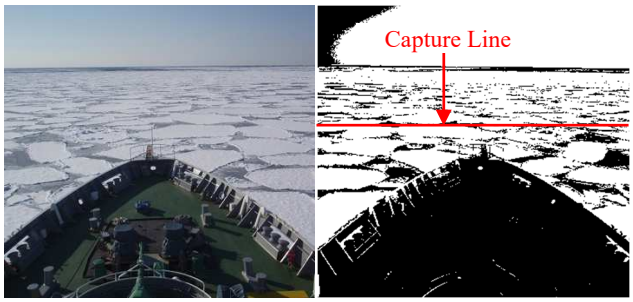

(a) (b)

Fig. 4 Example of captured video frame of front view (a) and binarized image (b) used for calculation of ice concentration

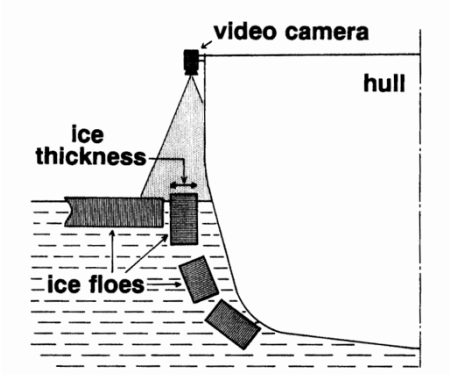

(a)

(b)

Fig. 5 Schematic diagram (a) and photo (b) of ice thickness observation by hull-side video camera (Shimoda *et al.*, 1997)

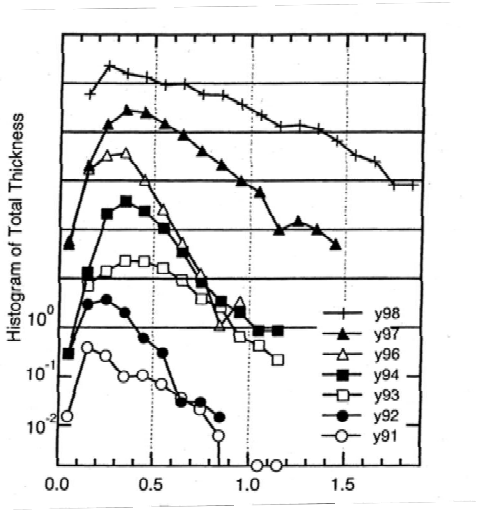

Fig. 6 Histogram of Total Thickness by Video Camera from 1991 to 1998 (Uto *et al.*, 1999)

Thick deformed ice, such as ridged ice, is one of the main concerns for ships in ice. In February 2004, NMRI introduced the ship-borne electromagnetic induction (EM) ice thickness observation technique. Figure 7 shows the principle of EM ice thickness measurement and its onboard installation. The EM sensor and the laser altimeter measure the distance to the ice bottom; Z_E and the distance to the snow surface; Z_L, respectively. Thus, the total thickness beneath the sensors; Z_I is calculated as:

$$Z_I = Z_E - Z_L$$

It enables us to continuously observe the thickness of ice, including ridged ice, with reasonable accuracy. Figure 8 shows the total thickness variation measured by the EM method during 2005-2009. Uto *et al.* (2006) proposed a method for improving the measurement accuracy of the thickness of ridged ice. The conversion algorithm from EM output to Z_E is developed by incorporating the internal structure model of ice derived from drill-hole measurements in the southern Okhotsk Sea. However, further research is required for the accurate measurement of the thickness of ridged ice.

By combining the above methods, we can continuously observe the ice condition along the ship track. Figure 9 shows an example plot between ice concentration by the video method and ice thickness by the EM method. Since the data sampling intervals are different between the two ways, all sampled data are averaged for each 2,000m advance of the ship. This plot helps overview the ice severity through voyages. In 2005 and 2006, the ice condition was relatively severe with thick ice, while it degraded after 2007. The ice concentration scatters similarly both in 2005 and 2007, however, the ship should experience more difficult navigation in 2005 due to the ice thickness of over 1.0m.

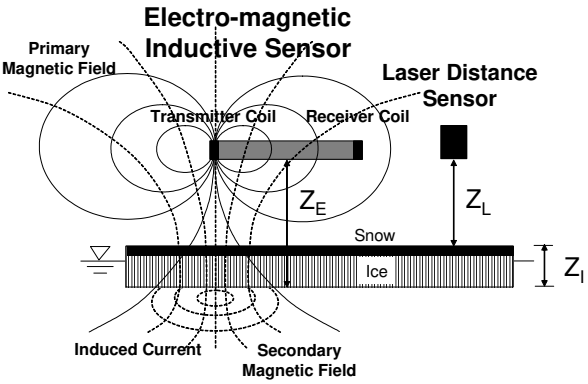

(a)

(b)

Fig. 7 Principle of EM sea ice thickness measurement technique (a) and EM equipment extended from the hull-side of P/V SOYA (b) (Uto *et al.*, 2006)

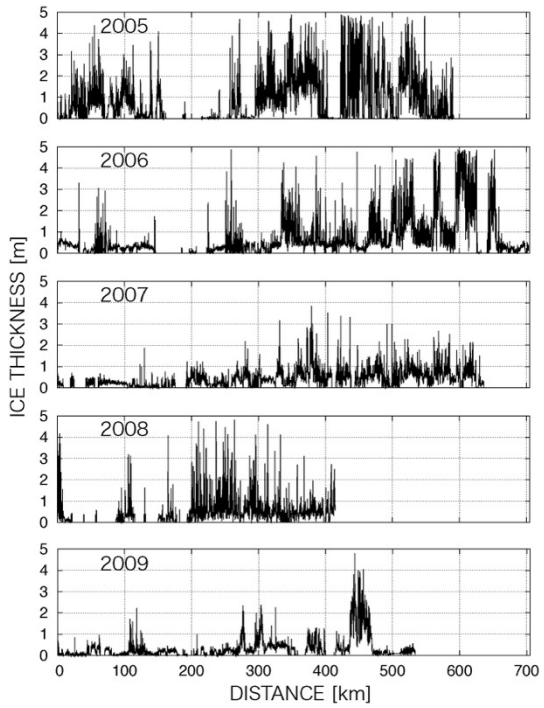

Fig. 8 Examples of total thickness measured by EM during 2005-2009 (Matsuzawa *et al.*, 2010a)

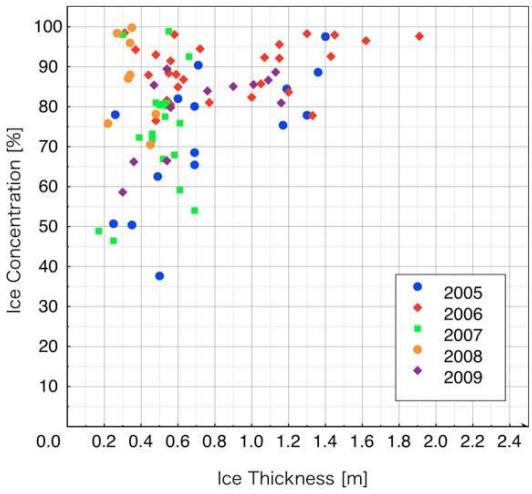

Fig. 9 Correlation plot between ice concentration and ice thickness during 2005-2009 (Matsuzawa *et al.*, 2010b)

4. Structural Response

Measuring hull ice loads is essential for evaluating the structural safety of ships in ice, and the results provide the base data for designing hull structures and structural requirements in ice-class rules. However, unlike the Baltic Sea, such data were rarely obtained in the Sea of Okhotsk.

Figure10 shows the installation of ice load measurements. Shear strain gauges were installed on frames of four sections at the bow and the bow shoulder. Two sets of shear strain gages were installed across the position where the ice load is expected to act. The strain gages were calibrated at least twice a day when SOYA stood for hydrographic survey or at night. The line load of ice acting on the hull was estimated using a couple of measured shear strains in respective frames. Ideally, the conversion factor from strain to load is obtained by physical calibration, such as pushing or pulling the hull. However, there was no such opportunity in the JSR. Thus, an FE analysis was carried out to obtain the conversion factor for each section.

During the ice load measurement, the video camera and the EM sensor synchronously recorded the ice concentration and the ice thickness, respectively. This measurement was conducted from 2005 to 2009. Figure 11 shows an example of the ice load at the bow section (Sec.2 in Fig.10(a)). The ice load estimated from the 2005 and 2006 measurements is plotted against the effective ice thickness. Here effective ice thickness is defined as the averaged ice thickness divided by the averaged ice concentration. The dotted lines in Fig. 11 indicate the design ice loads specified in the Finnish-Swedish Ice Class Rules. The observed results are well below the design ice load both at the bow and in the mid-part of the hull.

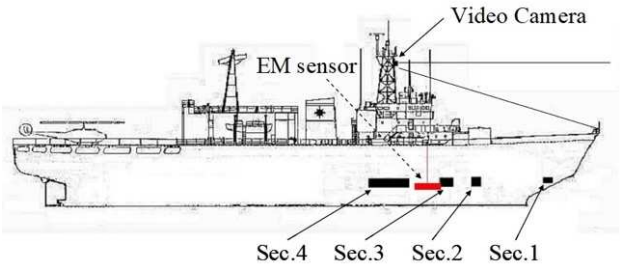

(a)

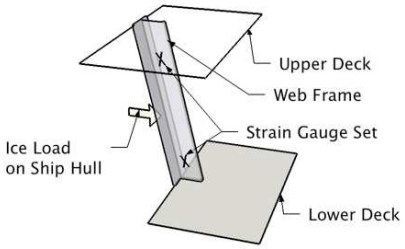

(b)

Fig. 10 Layout of ice load measurement instruments on P/V SOYA (a) and schematic of strain gauge installation on a frame (b) (Matsuzawa *et al.*, 2009)

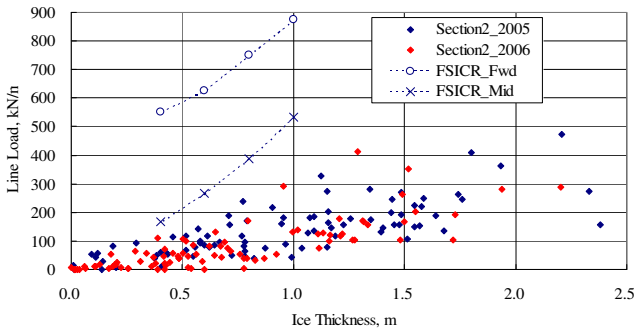

Fig. 11 Correlation between ice loads and effective ice thickness (Takimoto *et al.*, 2007)

5. Propulsive Performance

Various models and numerical simulations have been developed to evaluate ship resistance and propulsive performance in ice. To verify the validity of these models and simulations, collecting propulsive performance data in ice conditions is necessary. Thrust data is beneficial because it is comparable directly with estimated resistance. However, it is difficult to keep its measurement accuracy.

In the JSR, we installed strain gauges on the portside shaft and measured compressive and torsional strain (Fig. 12) to obtain thrust and torque. These measurements were conducted on cruises in 1997, 2011, and 2013. The shaft speed was measured by a photoelectric sensor. The CPP blade angle and ship speed were recorded by reading its indicator and a GPS, respectively.

Suzuki and Nakato (1990) reported the pros and cons of two strain-gauge configurations, i.e., "Conventional" and "Hylarides," used for the thrust measurement. In the JSR measurements, the "Conventional" method was adopted because it effectively eliminates thermal strains to compressive strain with a better S/N ratio. However, when using the configuration, a careful and precise setting of strain gauges was required because the angular misalignment of strain gauges results in the cross-coupling between torsional and compressive strains. The clockwise and counterclockwise shaft turning at a low rotation rate were conducted before the speed trial to obtain the correction factor for the cross-coupling effect.

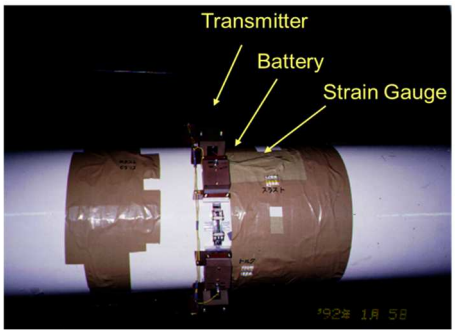

Fig. 12 Configuration of shaft output measurement

Uto *et al.* (1999) conducted an uncertainty analysis of the thrust measurement in February 1997. Figure 13 shows the results of the thrust measurement with the 95% confidence interval as an error bar. Thrust at a ship speed of approximately 4 knots in a 94 cm-thick ice was 386 ± 52 kN. The 95% confidence interval is within ± 13.5% of the average thrust. Removing the cross-coupling effect and minimizing the zero-drift resulted in relatively good accuracy for the thrust measurement.

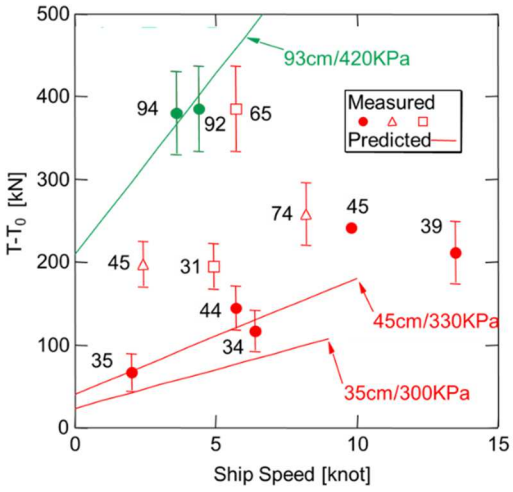

Fig. 13 Thrust vs. ship speed (Uto *et al.*, 1999). T denotes the raw thrust. T0 is the thrust measured at zero angles of CPP blades before speed trials. Both thrusts were measured on the port-side shaft.

Although many mathematical models and simulations are proposed, ice tank experiments are still acceptable as the most reliable method for predicting ship propulsive performance in ice. Thus, the model-ship correlation of propulsive performance in ice is one of the most critical tasks in the hull shape design of ice-going vessels. We conducted the resistance tests of a scaled model of P/V SOYA in level ice at the ice model basin of NMRI. The resistance model of P/V SOYA in level ice was derived from the regression analysis of experimental data. Thrust is calculated by dividing resistance with the thrust deduction factor.

Figure 13 plots the predicted thrust on the port-side shaft versus ship speed from ice tank experiments for a particular ice thickness and flexural strength. Here, the predicted thrust is halved, assuming both shafts share an equal thrust. It shows fair agreement between full-scale measurement and prediction by the model experiment.

Uto *et al.* (2015) proposed the hybrid model of resistance prediction for ships navigating in floe ice, such as small ice floes, large ice floes, and an ice-clogged channel. The accuracy of the model was validated through comparisons with the model-scale experiments conducted at the ice model basin of NMRI and the full-scale thrust measurements (Fig. 14). It is found that the proposed model can predict the resistance in floe ice of various sizes and concentrations with reasonable accuracy.

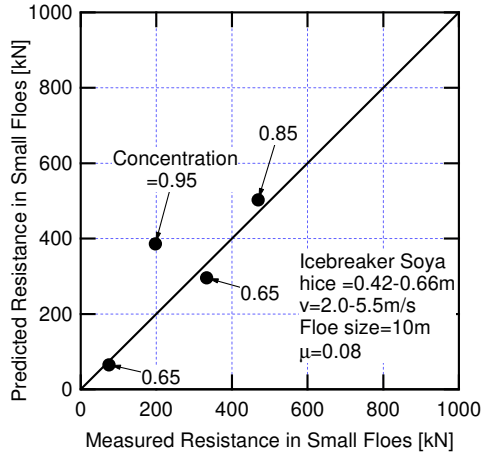

Fig. 14 Comparison of Resistance in Small Floes between Measured and Predicted (Uto *et al.*, 2015)

6. Conclusion

The results of the full-scale experiments conducted onboard the Japan Coast Guard patrol vessel SOYA in the Sea of Okhotsk off the coast of Hokkaido are summarized. The long-term data accumulation over more than twenty years would contribute to the design and operation of forthcoming patrol vessels of the Japan Coast Guard. Although it has been challenging to conduct such large-scale and long-term experiments in Japan in recent years, we conclude this article by pointing out the importance of taking every opportunity to obtain data from such experiments to advance ice engineering research.

Acknowledgment

We would like to express our deepest gratitude to the Ship Division of the Japan Coast Guard, the 1st Regional Coast Guard Headquarters, and the crews of the patrol vessels SOYA and TESHIO.

References

Institute for Low Temperature Science, Hokkaido University (1996-2022, annual): Sea Ice Research Activities by P/V Soya (in Japanese.)

Matsuzawa, T., H. Shimoda, D, Wako, T. Takimoto, and K. Izumiyama (2009): Measurement of Ice Load on the Ship Hull of P/V Soya. *Annual conf. of Japan Society of Naval Arch. Ocean Eng. 2009*, **9E**, 2009E-GS4-9, 155-158 (in Japanese.)

Matsuzawa, T., H. Shimoda, D. Wako, T. Takimoto, and K. Izumiyama (2010a): Transition in Five Years of Ice Thickness Measured by Ship-borne EM Sounding in the Southern Sea of Okhotsk. *Proc. 25th Int. Symp. on Okhotsk Sea & Sea Ice*, **25**, 81-84.

Matsuzawa, T., T. Takimoto, H. Shimoda and D. Wako (2010b): Five-year Observations of Ship Hull Ice Load in the Southern Sea of Okhotsk. *Proc. 20th IAHR Int. Symp. on Ice*; *Jun 14–18*, *Lahti*, *Finland*.

Shimoda H., T. Endoh, K. Muramoto, N. Ono, T. Takizawa, S. Ushio, T. Kawamura, and K.-I. Ohshima (1997): Observations of Sea-Ice Conditions in the Antarctic Coastal Region Using Ship-Board Video Cameras, *Antarctic Record*, **41**, **1**, 355-365 (in Japanese.)

Suzuki T. and M. Nakato (1990): Thrust Measurement Technique in Sea Trial Conditions: Assessment and New Development. *Proc. PRADS'92*, *the 5th International Symp. on the Practical Design of Ships and Mobile Units*, **1**, p.1403.

Takimoto, T., S. Kanada, H. Shimoda, D. Wako, S. Uto, and K. Izumiyama (2007): Ice Loads on Ship Hulls in Pack Ice Conditions. *Proc. POAC2007*, *the 18th Conf. on Port and Ocean Engineering under Arctic Conditions*, **1**, 267-276.

Takimoto, T., S. Uto, D. Wako, K. Izumiyama, S. Kanada, and H. Shimoda (2008): Full-Scale Measurements of Local Ice Load on Ship Hull in Pack Ice of the Southern Sea of Okhotsk. *Proc. Oceans / Techno-Ocean 2008.*

Uto S., K. Tamura, and S. Narita (1999a): Consideration on Accuracy of the Full-scale Thrust Measurement in Ice by Strain Gauges. *Proc. 18th International Conf. on Offshore Mechanics and Arctic Engineering*, OMAE99/P&A-1109.

Uto S., H. Shimoda, and K. Tamura (1999b): Ship-based Sea Ice Observations in the Southernmost Part of the Sea of Okhotsk. *Proc. 15th POAC'99*, 380-388.

Uto S., H. Shimoda, D. Wako, and T. Matsuzawa (2015): NSR Transit Simulations by the Vessel Performance Simulator "VESTA" Part 2 Simple Resistance Formulae of Ships in Floe Ice. *Proc. 23rd POAC'15.*

Uto, S., T. Toyota, H. Shimoda, K. Tateyama, and K. Shirasawa (2006): Ship-borne Electromagnetic Induction Sounding of Sea Ice Thickness in the South Okhotsk Sea. *Ann. Glaciol.*, **44**, 53-61.

Correspondence to: T. Matsuzawa, zawa@m.mpat.go.jp

Okhotsk Sea and Polar Oceans Research 7 (2023) 13-16

https://doi.org/10.57287/ospor.7.13

Article

The Northern Sea Route: A review of recent developments

Arild MOE[1]

[1]*Fridtjof Nansen Institute, Lysaker, Norway*

(Received September 24, 2022; Revised manuscript accepted October 31, 2022)

Abstract

The Russian president and government have over the last 10-12 years expressed high ambitions for development of NSR. International transit shipping has not taken off, but destination shipping has increased radically in recent years, primarily transportation of liquefied natural gas from the Yamal peninsula. Organization of the shipping activities initially involved consortia of international shipping companies, but Russian policies have later taken a protectionist direction. Russia introduced regulations mandating that all oil, liquefied natural gas and coal loaded from within the Northern Sea Route area can only be transported on Russian-flagged ships; and from 2019 transportation of hydrocarbons out of the NSR area would be reserved for vessels built in Russia. The administration of the sea route has recently been changed; all key functions are now concentrated in Rosatom – the mother organization of the nuclear icebreaker fleet. The war in Ukraine creates uncertainty about further development of the sea route as very much depends on the fate of the hydrocarbon projects expected to be the base load of traffic. Technology sanctions, investment restrictions and limitations on market access are likely to slow down their development. This is also likely to affect the very expansive icebreaker construction program.

Key words: Arctic, shipping, LNG, Rosatom, icebreakers, Russia

1. Introduction

The Northern Sea Route (NSR) is the Russian term for the waterways north of Siberia. They form a part of the Northeast passage (NWP), which is the historical term for the Arctic Sea passage between the Atlantic and the Pacific. Whereas NWP is a loose term, without strict geographical boundaries, the NSR is now precisely defined in Russian law since 2013 as an area starting with the entry to the Kara Sea and stretching all the way to the Bering Straits. Northwards it extends to 200 nautical miles from the coast (Fig. 1). Russia maintains it has a right to manage traffic in this area based on article 234 of the Law of the Sea Convention, as well as historical rights. The Russian position is contested by some other states, notably the United States.

Fig. 1 Map of the Northern Sea Route

In this article I will discuss recent developments in the use of NSR and the administration of the sea route, as well as briefly assess outlook in light of Russia's war in Ukraine.

2. The revival of NSR

The Russian president and government have over the last 10-12 years expressed high ambitions for development of NSR and the administration of the sea route underwent a significant overhaul in 2010-2013 designed to attract traffic. Application procedures were simplified, and icebreaker escort fees became negotiable (Solski, 2020).

For some time, there were expectations that international transit shipping would take off. But it did not happen. Other developments were more encouraging, though. Several large extraction projects in northwestern Siberia were initiated, requiring transportation by sea of heavy machinery and materials – and shipment of resources out of the region when the projects came on stream. This is destination shipping. With the successful start of the Novoportovskoye oil project in 2016 and the Yamal-LNG project in 2017, total cargo volume on the NSR increased rapidly and has hovered around thirty million tons the last few years (Gunnarsson & Moe, 2021) (Fig. 2).

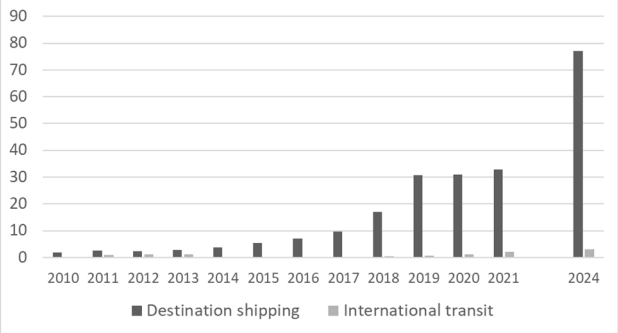

Fig. 2 NSR Cargo volume 2010-2021 and target 2024. Million tons.

The owners of the Yamal LNG plant with the Russian gas company Novatek in the lead set up a scheme where consortia of international shipping companies were invited to invest in icebreaking LNG carriers designed for Yamal LNG built in Korea against long term contracts for transportation of gas (Table 1).

Table 1: Icebreaking LNG carriers constructed for Yamal LNG

Name	Operator
Christoph de Margerie	Sovcomflot
Boris Vilkitsky	Dynagas
Vladimir Rusanov	MOL
Fedor Litke	Dynagas
Eduard Toll	Teekay
Rudolf Samoylovich	Teekay
Vladimir Vize	MOL
Georgiy Brusilov	Dynagas
Boris Davydov	Dynagas
Nikolay Zubkov	Dynagas
Nikolay Yevgenov	Teekay
Vladimir Voronin	Teekay
Nikolay Urvantsev	MOL
Georgiy Ushakov	Teekay
Yakov Gakkel	Teekay

(Source: Reuters)

The carriers are all of the same design;
Capacity 170 000 m^3 LNG,
Length: 300 meters,
Ice class: Arc7, can break 2.1 meters of ice.

Except the carrier operated and owned by Sovcomflot they are all owned by international shipping consortia where Chinese shipping companies are partners.

It looked like the development of Arctic LNG would become a truly international endeavour, since also the LNG plant itself had substantial foreign ownership shares (French and Chinese).

3. End of the international phase?

In 2018, Russia introduced regulations mandating that all oil, liquefied natural gas and coal loaded from within the Northern Sea Route area can only be transported on Russian-flagged ships to the first point of destination or transshipment. More restrictions were proposed soon after: From 2019 transportation of hydrocarbons out of the NSR area would be reserved for vessels built in Russia (Federal Law, 2017).

This was part of a concentrated effort to support the ailing Russian ship-building industry, as well as finding business for the giant shipyard Zvezda under construction in the Far East. It was, however, impossible to implement this policy in full at a time when the extracting companies needed a series of new carriers and tankers over a short period. Thus, exemptions were made, and Korean yards continued to play an important role. But the signal was clear. Russian shipping policies were becoming more protectionist.

4. A new boss for the NSR

Except for the LNG, the traffic development was not as brisk as Russian authorities hoped for, and this was one reason why the government searched for a new model for management of the sea route. It argued that better coordination of operations and investments was needed. After a protracted institutional battle, the State Russian nuclear power corporation – Rosatom, the mother organization of the nuclear icebreaking fleet - was named “infrastructure operator” of the NSR from 2019. (More detail in Moe, 2020a).

It was first decided that it should share responsibilities with the Ministry of Transport. The Ministry would be responsible for development of laws and regulations and control their implementation and also issue permits for entry to the sea route area. Rosatom would take control over current operation of the sea route, and, crucially, manage state property and assets in ports, in addition to the icebreakers. Disputes about the control of key activities such as navigational and hydrographical support continued, however. By August 2022, it appeared that Rosatom had won this battle completely and pushed aside the Ministry when it also took over the issuing of navigation permits. All functions will now be concentrated in one structure under Rosatom - The Main directorate of the Northern Sea Route – Glavsevmorput – same name as the state structure that governed NSR in the 1930s (Atomnaya energiya, 2022).

The aim of the NSR reform has been to increase harmonization and efficiency. A counter argument is that with the new structure there is a risk that Russia’s Arctic

economy will become even less transparent than it has been, with cross subsidization within the giant Rosatom, and that this will negatively affect economic effectiveness. Another question is the strength and independence of regulators.

But the last step in Rosatom's takeover of ministry functions was in fact justified by operational and safety issues. In November 2021, 24 ships were trapped in the ice, ostensibly due to poor coordination of permits, icebreaker assistance and instructions given to captains. Settlements and industrial projects suffered (Strana Rosatom, 2022).

Many will find it problematic that Rosatom is a de facto monopoly provider of icebreaker services as a business at the same time as it is the state authority. In addition, Atomflot is starting to offer freight services, in competition with ordinary shipping companies (Moe, 2020a).

5. Russian ambitions and the outlook

The ambitions for further growth in traffic has been high, crystallised in President Putin's 2018 declaration of transporting altogether 80 million tons of cargo on the NSR by 2024. Officially, the target is still to transport 120 million tons by 2030. The main component of this cargo base was expected to be LNG from a series of new projects in the vicinity of Yamal LNG plus a giant oil project – Vostok Oil – under development further east, near the Siberian shore.

After the Russian invasion of Ukraine with ensuing economic sanctions against Russia and further turmoil, the build-up looks impossible. LNG projects are already delayed because of technology sanctions; investment squeeze and uncertain market access is also expected to slow down industrial projects in the Russian Arctic. This also puts a question mark over the ambitious plans for renewal and expansion of the nuclear icebreaker fleet. As of 2022, five such icebreakers were in operation, two were under construction, one of them almost finished, concrete preparation for three more had been made, and plans for two more had been announced. The last three would be of the Leader model. It is a 120 mega-watt vessel, twice as strong as the most powerful icebreaker today. It has been designed with the objective of keeping the sea route open all year and facilitate LNG exports directly to Asia, also in the winter (Moe, 2020b). The icebreakers are very costly, if the outlook for hydrocarbon exports changes, the economics of the icebreaker program is undermined. But of course, also the need for new icebreakers will have to be reassessed.

References

Atomnaya energiya (2022). В Росатоме создано Главное управление Северного морского пути - «Главсевморпуть» [In Rosatom a Main directorate for management of the Northern Sea Route has been created- Glavsevmorput] 5 August. https://www.atomic-energy.ru/news/2022/08/05/127067?ysclid=l8ag90zguc668828606

Federal Law (2017). "О внесении изменений в Кодекс торгового мореплавания Российской Федерации и признании утратившими силу отдельных положений законодательных актов Российской Федерации." [About amendments in the Code for merchant navigation and recognition of expiration of some provisions of legal acts of the Russian Federation] No. 460.F3. Rossiyskaya gazeta, 31 December. https://rg.ru/2017/12/31/fz-460-dok.html

Gunnarsson, B., & Moe, A. (2021). Ten Years of International Shipping on the Northern Sea Route: Trends and Challenges. *Arctic Review*, 12, 4-30. https://doi.org/10.23865/arctic.v12.2614

Moe, A. (2020a) A new Russian policy for the Northern Sea Route? State interests, key stakeholders and economic opportunities in changing times. *The Polar Journal,* 10:2, 209-227, DOI: 10.1080/2154896X.2020.1799611

Moe, A. (2020b). Russian Policies for Development of the Northern Sea Route: An Assessment of Recent Developments and Implications for International Users. In Lawson Brigham et. al. (eds). *The Arctic in World Affairs: Will Great Power Politics Threaten Arctic Sustainability?* 2020 North Pacific Arctic Conference Proceedings. Published by Korea Maritime Institute, Busan, Republic of Korea and East-West Center, Honolulu.

Solski, J. (2020). The Northern Sea Route in the 2010s: Development and Implementation of Relevant Law. *Arctic Review*, 11, 383–410. https://doi.org/10.23865/arctic.v11.2374

Strana-Rosatom (2022). Главсевморпуть: новые возможности с опорой на исторический опыт [Glavsevmorput: New possibilities anchored in historical experience]. 7 July. https://strana-rosatom.ru/2022/07/07/glavsevmorput-novye-vozmozhnosti-s-o/?ysclid=l8a9ozfejr110177343

Summary in Japanese

和文要約

北極海航路：最近の現状

Arild MOE [1]

[1] フリチョフ・ナンセン研究所、ノルウェー

ロシア政府が定める北極海航路(NSR)の現状概要を述べた。アトムフロートは NSR に係る全権をほぼ掌握するも砕氷船不足の問題は解消するに至らず、また、造船のロシア自前産業への移行を目指す政策には確たる進展がなく、砕氷 LNG 船団構成にも変化が見えない。ウクライナ問題を抱え、NSR の今後の見通しは定かではない。

Correspondence to: Arild Moe, amoe@fni.no

Okhotsk Sea and Polar Oceans Research 7 (2023) 17-21

https://doi.org/10.57287/ospor.7.17

Article

Towards the Conceptional Design of Coastal Wave Database around the Sakhalin Island

Vitaly KUZIN[1] and Andrey KURKIN[1]

[1]*Nizhny Novgorod State Technical University n.a. R.E. Alekseev, Nizhny Novgorod, Russia*

(Received October 28, 2022; Revised manuscript accepted December 29, 2022)

Abstract

The present article describes the observation system and the outline of recorded data of the field experiments carried out in the Sea of Okhotsk, mainly at the coast of the Sakhalin Island in 2016-2019. LMNAD (Laboratory of Modeling of Natural and Anthropogenic Disasters) conducted a series of field experiments and meteorological observations. The coastal wave data were obtained by the instrument system developed by the authors' group, taking account of the shallowly longshore. The article also mentions the unique instrumentation, stepwise developed autonomous wave recorder.

Every wave recorder's data was transmitted to the onshore center by electrical devices. Before too much data collected, the authors should think about the database, for instance, whether the database is of international format or of regional one, and necessity of a datacenter. In a decade to come, the database will remain a regional one. When the data grow up to a long-term dataset of coastal wave around the Sakhalin Island, the database would probably be extended to the internationally available data. The present article notes an initial stage of a conceptual design of a coastal wave database around the Sakhalin Island, for the moment, which was composed of the data of the field experiments carried out in the Sea of Okhotsk in 2016-2019.

Keywords: coastal zone, monitoring, wave characteristics, data collection, database

1. Introduction

Due to everlasting activities of the industries in survey and extraction of oil and gas in the shelf area around the Sakhalin Island, the necessity of reliable assessment of costs of the construction of the shore and offshore infrastructures arises. Together with it, the safety in their constructions and installations of the infrastructures has been more strictly and widely appreciated. The climate and oceanographical information in this area are vital for both.

The present paper describes the approaches to respond these demands with the use of software and hardware measures of observations, for instance, by a systematically developed autonomous mobile system equipped with a group of sensing devices. The paper also mentions the outline of the field experiments conducted in the vicinity of the Cape Svobodni in Mordvinova bay of the Island of Sakhalin, in 2016-2019, and the algorithms of processing of recorded data through the experiments. Currently, there are several methods of monitoring sea ice environment and wave climate in the coastal zone of the Sakhalin Island [Kurkin *et al.* 2017]. The observation of remote-sensing image of satellites is one of them. However, in this area, those data possess significantly lower resolution compared to aerial survey data in the field and are often poor under the conditions of dense cloud coverage and other adverse weather conditions.

Observations with the use of aircrafts and/or unmanned drones covering the whole target area would be another way, only if their easy operations be established on a financial and safety footing. The financial and personal supports, including AI producers, will absolutely be necessary for the microwave satellite system.

In this context, the platforms, that are, ground-vehicles patrolling along the water area to monitor sea ice conditions and wave climate were utilized during the field experiments in 2016-2017 [Kurkin *et al.* 2016–2017 (AMRK)].

Remote sensing methods, that are currently used, are the appropriate methods of coastal zone research. To transmit the senor data to the onshore center, transducers and/or wide-range lasers are utilized.

A serious problem lies on the onshore center. The sizes of the onshore centers need usually about several square meters. The centers demand very high electric power and must be set up at high and stationary place.

It can be said that the centers are handicapped by their high-cost facilities.

Before too much date collected, the concept of the database must be discussed, and a conceptual design of the database should be initiated through considerations of easiness of dealing with and

accessibility to the database, and trustworthiness. Current states of the database design are briefly noted.

2. Field experiments

Field experiments were performed at the shore of the Sea of Okhotsk in 2016-2019, applying various instruments, mostly the platforms which are unmanned ground-mobile multi-purpose units with the capability of transmitting many measurement data of wave climate in the coastal zone.

During the experiments performed in 2019, a system of telemetry and evaluation of wave and meteorological climate in the coastal zone was tested with the use of the autonomous measurements system, which was integrated into a unified information network. Marine-based radiolocation station (FURUNO FAR, RLS Mikran), meteorological station with the autonomous power source (VIOSALA) supported their consecutive work during the whole experiments and assisted well in the transmission of self-made blocks of the measured data by hydrodynamic pressure sensors in shallow water near the shore.

3. Observation system

The instrumentation was composed of an integrated autonomous unit. The software and algorithm were developed for the purpose of control, registration, and comparison of the data. The next chapter describes the outline of this system and the software for correlation of the data obtained from various devices with the use of the sensor-fusion technology, which is still under development.

As noted in Chapter 2, the radar station, Mikran "River" RLS (Mikran "Reka" RLS) was recognized as an effective element in the field work.

"Reka" «River» is a highly technological radio navigation system, particularly in river transport field, which can monitor and control a navigation situation at every moment. Based on the state-of-the-art broadband signal technology, digital solid state transmit/receive module ensures a highly accurate target detection and identification even of small-sized objects like people, sea ice floats, buoys, etc., in any weather conditions. With this exclusive technology, a radio navigation system REKA has been designed, manufactured, and tested in viewpoints of performance, reliability, and quality requirements, compatible with compass, echo sounder, GPS, AIS, etc.

The measurement system was composed of the following units.

a) Mikran "River" MRS-1000 radiolocation station. The operational frequency of RLS was 9500 MHz, wavelength 3 cm, and horizontal polarization. The range resolution was 3 m in the direction angle of 1°. Rotation speed of RLS was 24 rpm, and discrete period was 2.5 seconds.

b) Vaisala WXT520 meteorological station did the duty of measuring wind speed and direction, ambient air temperature, relative humidity, atmospheric pressure, and amount of precipitation.

c) GPS with a positioning system.

The measurement platform was equipped with the following devices

a) Self-made watertight case with a set of hydrodynamic pressure sensors; maximum measurement frequency was 13 kHz.

b) Submerged hydrodynamic pressure sensors with an anchor, installing RLS's field of view in the specified range from 30 to 60 degrees (to avoid the shadows from the buildings on the shore).

Fig. 1. Ray tracing scheme of the Mikran "River" RLS during the experiment conducted in Cape Svobodni in 2019

The cooperations of the multi-agents in the Sakhalin Island created the formation of radiolocation scan system in 2019. Brief scheme of RLS installation is shown in Figure 1.

RLS emitter covered the horizontal detection area from 30 to 60 degree and from 500 to 1000m from the emitter point.

Self-recording quartz pressure transducer APB-K14 was used to determine the water pressure at the point of observation. This device provides the sea level parameters, sea wave height, with a high resolution in real time, and transmits the data through the connected cable system. The transducer APB-K14 is equipped with quartz pressure and temperature transducers, as well as output for external device control. However, when such transducers are used in the field, their backgrounds should be reminded.

By the quartz transducer, pressure and temperature are converted into electrical signals, where quartz crystal will oscillate at a particular frequency when a driving signal is applied to the crystal. As physical properties of

the crystal change, because of changes in temperature and pressure, the oscillation frequency changes. In quartz transducers, the oscillation frequency is measured and converted to electrical signals which vary as the pressure and temperature applied to the crystal varies. APB-K14 equips with an automatic checking unit.

While the transducer APB-K14 was installed in stationary mode on the bottom of the sea or fixed at a certain depth of water, the transducer provided the wave climate data during the whole period of the observation. The data were collected and extracted for the analysis of wave parameters.

For the present, both of remotely obtained data (Table 1) and on-site data (Table 2) of coastal waves were recorded and stored in a temporary data file. As clearly shown in Table 1, the remotely measurements contain a difficulty in carrying out calibrations of the recorded data.

Table 1. Equipment for remotely measurements

Measurement type	Equipment	Measurement items	Disadvantages
Ground-based sounding	Radio detecting and ranging equipment (RLS)	Wave height, speed and direction of flow, surface wind	Calibration of devices with the use of real data is required
	Lidar system	Pollution of water environment and the coast, wave breaking	Calibration of devices with the use of real data at the certain point of research is required Low range of operation (compared to RLS)
Aviation sounding	Radiolocation device	Speed and direction of flow, surface wind speed	Inability to conduct continuous long-term research in the chosen field. Calibration of devices with the use of real data is required
Satellite sounding	Altimeter	Ocean surface altitude, surface wind, wave height. Film contamination	Inability to conduct continuous long-term research in the chosen field. Calibration of devices with the use of real data is required
	Radiolocation synthesis of the aperture	Film contamination, surface wind, wave height.	

On the other hand, the in-situ measurements also have weaknesses. The area of measurements is limited (Table 2). Together with them, as most of the measurement devices require their power sources. The autonomous mobile measurement platforms will relatively be superior in operations of long-term wave climate research in the remote areas of the coast, even at hard-to-reach locations.

In-situ experiments, subaqueous pressure sensor was installed in the sensor system, for the necessity in correlation with the RLS operation and by comparison of the intensity of reflected signal with the right data of wave height in a certain point [Young *et al.*] Submerged hydrodynamic pressure sensor installed on the sea bottom with a weighting attachment was used to compare the intensity of the reflected signals with those of the real wave height.

Taking account of the development in hardware and software systems for observations and analyses of sea wave climate, the utilization of the autonomous mobile platforms will currently be relevant. This system is capable of evaluations of the wave climate of the remote areas in the coastal zone as mentioned above.

For the moment, an easy-handling data storage system is vital for the long-term coastal data, both of wave and meteorological ones, while the authors are giving thorough consideration to the final data format.

Table 2. Equipment of on-site measurements

Equipment	Measurements	Disadvantages
Floating beacon with an accelerometer	Statistical and spectral characteristics of waves, velocity and direction of the wind, velocity of the flow	Small area measurement Possibility of losing the device
Floating beacon with a hydrostatic pressure sensor		
Floating beacon with a hydrometric flowmeter		
Subaqueous pressure sensor	Wave height, flow velocity	Small area measurement There is no real-time data transfer in the autonomous systems. Possibility of losing the device
Acoustic pressure sensor	Wave height, flow velocity	Small area measurement There is no real-time data transfer in the autonomous systems. Possibility of losing the device
Capacitive wave gage	Wave height	Point measurement Construction fragility
Resistive wave gage		

The autonomous mobile platforms, equipped with sensor arrays, have a capability of performing panoramic

observations of environmental phenomena in the coast, as well as in the flooded zones. The systems are appropriate for a long-term installation through being capable of recording uninterrupted data and the ability to cover the observation areas at several hundred meters away from the shoreline, which can pursue research in the coastal zone at any time and beyond the initial scope. However, it should be noted that the trustworthiness of the data received via the contact method of floating beacons, capacitance wave gages, and subaqueous pressure sensos depends on the natural conditions at the time of measurements [Rodin *et al.* 2016].

4. Data visualization

Self-made software (the development is in progress) can read the recorded dump files of the performed experiments and select separate snapshots of analyzed intensity as the results of RLS operation. The software is also capable of extracting the data package in the format in accordance with the following specification:

Specification:

The cartesian file data contains Cartesian coordinates and intensity. The columns are written in the following order: X coordinate, Y coordinate, I signal strength.

The polar file data contains the polar coordinates of the current segment together with signal strength. The columns are written in the following order: R vector (radius and the number of readings on the beam), angle Φ, I — signal intensity.

APB-K14, with its hardware and software, by using RLS calibration factors, provided the visualized data, as shown in Fig.2. The procedure of producing significant wave heights require the RLS calibration factors. The procedure does not much time for the processing.

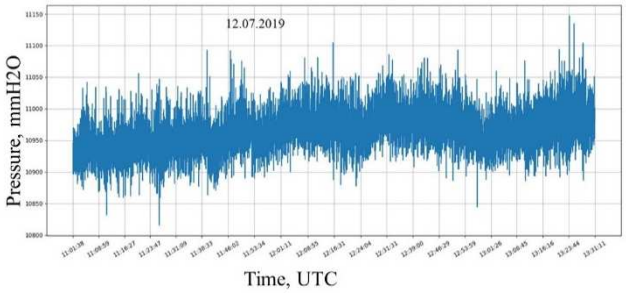

Fig. 2. Example of APB-K14 data visualization

The observation system was set up in stationary mode on the bottom of the sea or fixed in water layer and providing coastal data during the whole period of research. The coastal wave data parameters were extracted from the recorded data and analyzed.

Visuization procedure generates the dump file, about 6-10 GB in the present case. Juts for an example, Fig.3 shows visualized dump files of the Mikran RLS. Cape Svobodni case in 2019.

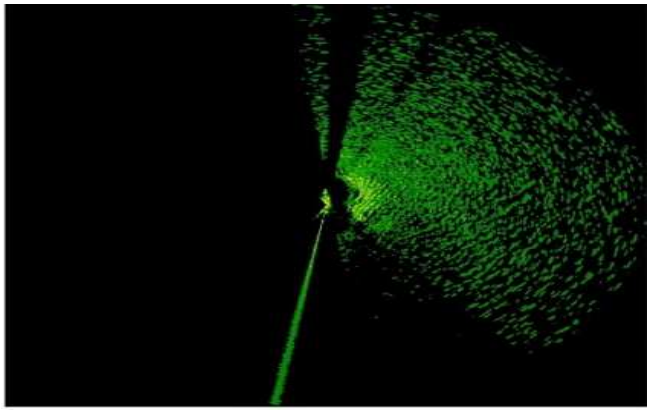

Fig. 3. Visualization of dump files recorded during the experiments of recording the Mikran "River" RLS. Cape Svobodni, 2019.

5. Conceptual design of the database

A database is indispensable through the visualization procedure of coastal wave, although it might simply be an easy-handling one.

We live in an age when the most of information are transmitted and exchanged each other in wireless systems. The coastal wave data around the Sakhalin Island obtained by bearing hardship should be accessible to any person's and organization's demands with relation of the other data.

A relational database has been used in a wide range of data and is rated it matured and reliable. Especially, a well-designed database will enjoy several benefits and strengthen it with other big database such as the World Ocean Database (WOD) that is world's largest collection of uniformly formatted, quality controlled, publicly available ocean profile data. The authors find the prospect of the relational database. The relation with the WOD will raise up the authors' database to the larger one, which will lead to apply the machine learning tool, and even deep learning in future. The deep learning would be able to improve the accuracy of satellite microwave sensing data.

The initial database composes of the materials for 2016-2017 on coastal wave climates.

6. Conclusion

The authors described the approaches to respond scientific and technological demands around the Sakhalin Island with the use of software and hardware measures of observations. In particular, the systematically developed autonomous mobile platforms equipped with sensor arrays worked well. The field experiments performed with those platforms were finished successfully in the vicinity of the Cape Svobodni in Mordvinova bay of the Island of Sakhalin, in 2016-2019. The authors confirm that the algorithms of

processing of recorded data through the experiments operated well. A large amount of oceanographical and meteorological data were obtained and preserved in the storage files.

In the case of extremely high waves, stormy weather, and especially high and low tides, the platforms were found useful. Two normative modes, summer-mode, and winter- mode, are arranged for the platforms.

To respond rapidly advance in marine observation technology, further developments of instrumentation and algorithm have been planned. The first term will begin early in 2023.

The stored materials should be publicly available coastal marine profile data. World Ocean Database is good guide to establishment of the coastal Sakhalin Island database, as the WOD is one of the largest and trustworthy relational databases.

The authors has just stood at the starting point of composing the relational database of the coastal marine climates around the Sakhalin Island.

Acknowledgements

This research was funded by the grant of the President of the Russian Federation for state support of Leading Scientific Schools of the Russian Federation (Grant No. NSH-70.2022.1.5.).

References

Kurkin A. and 3 co-authors (2017): Unmanned ground vehicles for coastal monitoring. *International Journal of Imaging and Roboics,* 17(1), 64-75.

Zaytsev A. and 11 co-authors (2017): Coastal monitoring of the Okhotsk Sea using an autonomous mobile robot. *Science of Tsunami Hazards*, 36(1), 1-12.

Kuzin V. and 6 co-authors (2018): Multi-robot system for monitoring ice and wave climate in coastal zone. *Proceedings of the 33rd International Symposium on Okhotsk Sea & Polar Oceans.*

Rodin A., I. and 2 co-authors (2016): Numerical study for run-up of breaking waves of different polarities on a sloping beach. *Extreme Ocean Waves*. Ed. E. Pelinovsky and C. Kharif. Switzerland Springer Int. Publishing, 155-172.

Kurkin A. and 3 co-authors (2020): Hardware-software complex for estimation of surface wave characteristics in the coastal zone. *Proceedings of the 35th International Symposium on Okhotsk Sea and Polar Oceans.*

Kurkin A. and 7 co-authors (2018) Development of a group of mobile robots for conducting comprehensive research of dangerous wave characteristics in coastal zones. *Science of tsunami hazards. V. 37. No. 3. P. 157-174.*

Ivonin D.V. and 4 co-authors (2016) The capabilities of x-band radar navigation systems for monitoring coastal wind waves. *Oceanology, vol. 56, no. 4, p. 647–658.*

Young I. and 2 co-authors. (1985) A three – dimensional analysis of the marine radar images for the ocean wave directionality and surface currents J. *Geophys. Res. V. 90. № C1. P. 1049-1059.*

Nieto Borge J.N. and 2 co-authors (1999) Estimation of the significant wave height with X-band nautical radars. *Proc. 18th int. Conf. Offshore Mechanics and Arctic Engineering (OMAE).*

Correspondence to: V. Kuzin, chromium32@mail.ru.

白ページ

Okhotsk Sea and Polar Oceans Research 7 (2023) 22-29

https://doi.org/10.57287/ospor.7.22

Article

On the Seasonal Variations of the Bering Slope Current

Humio MITSUDERA[1], Youichi HIRANO[2], Hatsumi NISHIKAWA[3] and Hung Wei SHU[4]

[1] *Institute of Low Temperature Sciences, Hokkaido University, Sapporo, Japan*
[2] *Graduate School of Environmental Science, Hokkaido University, Sapporo, Japan*
3 Atmosphere and Ocean Research Institute, University of Tokyo, Kashiwa, Japan
4 Japan Fisheries Research and Education Agency, Kushiro, Japan

(Received November 6, 2022; Revised manuscript accepted January 2, 2023)

Abstract

Seasonal variations of the Bering Slope Current (BSC) and eddies were discussed by analyzing an ocean general circulation model output. The model simulates the seasonal variations of the BSC realistically, in which the BSC flows along the shelf break over the slope in winter, and moves off-slope during spring and summer. Eddies start growing in winter, resulting in the BSC's separation from the shelf-break. The eddies grow as a result of baroclinic instability owing to the deepening of the main pycnocline of the BSC in winter, which is likely to be affected remotely by the deepening of the Alaskan Stream in the Gulf of Alaska.

Key words: Bering Slope Current, eddies, baroclinic instability

1. Introduction

The Bering Sea located between Siberia and Alaska. While the northeast portion of the sea is a wide and shallow continental shelf, its deep portion of the sea is divided into three connected deep basins and the largest one is the Aleutian Basin (Fig. 1 upper panel). The Bering Slope Current (BSC) flows over a steep slope that connects the continental shelf and the deep basin (Fig. 1 lower panel). The BSC is known as the Green Belt where the biological production is active throughout the year (Springer *et al.*, 1996). It was suggested that the high biological production would be supported by mixing along the BSC between nutrients originating in the deep basin and iron from sediments over the shallow continental shelf due to tidal mixing and eddies (*e.g.* Tanaka *et al.*, 2017).

The BSC exhibits distinct seasonal variations observed by satellite altimetry (Ladd, 2012). During winter, the BSC is strong and tightly confined to the continental slope. The BSC starts broadening and moves off-slope during spring and reaches the deep basin in summer. It appears that anticyclonic eddies drive the evolution of the BSC; the eddies grow during spring when the BSC moves off slope, and are matured in summer when the BSC reaches the deep basin (Ladd, 2014; Okkonen, 2001; Mizobata *et al.*, 2002). These anticyclonic eddy generation is likely associated with shelf-break canyons called Navarin Canyon, Zhemchug Canyon, and Pribilof Canyon (Fig. 1 lower panel). However, it is not known why the BSC exhibits such a distinct seasonality as described above and its relationship with eddies. Specifically, the questions are:

- Why does the BSC move from the slope into the deep basin during spring?
- How do eddies form and grow? What are roles of eddies in the BSC evolution?
- What are the energy sources of the seasonal evolution of the BSC?

We addressed these questions by analyzing an ocean model output by Matsuda *et al*. (2015).

2. Data

The model output by Matsuda *et al.* (2015), based on an ice-coupled ocean general circulation model (OGCM) developed at the Atmosphere and Ocean Research Institute, the University of Tokyo, was used to analyze the BSC. The horizontal coordinates is finer than 3km in the northwestern continental shelf in the Sea of Okhotsk, while it becomes approximately 10 km in the Bering Sea (Matsuda *et al.*, 2015). Vertically 7 sigma coordinate grids were arranged shallower than 35m, under which 77 level coordinates are assigned. This model adopts the turbulence closure scheme (Noh and Kim 1999) to simulate the evolution of the oceanic surface and bottom boundary layers. Ocean and sea ice were driven by atmospheric forcing calculated from Ocean Model Intercomparison Project (OMIP) Ver. 6. The tidal forcing of the K1 is applied to the momentum equation. Readers may find detailed information on the model in Matsuda *et al*. (2015).

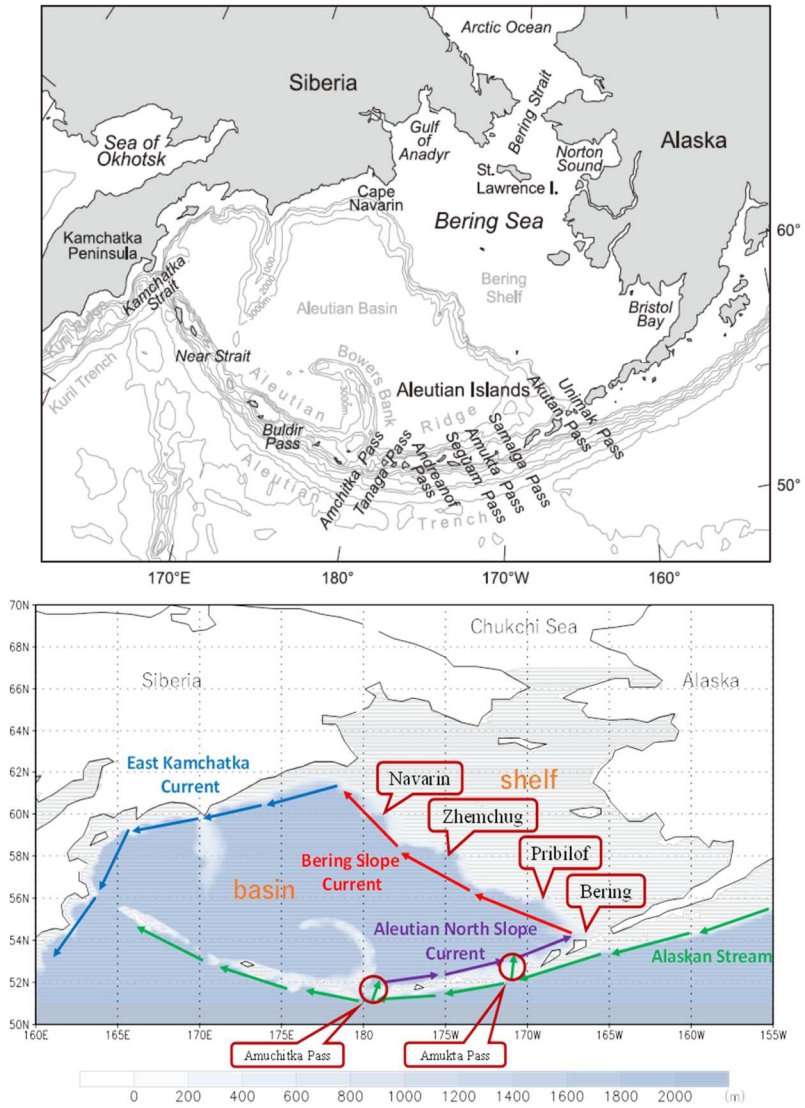

Fig. 1 (Upper) Geography of the Bering Sea (adopted from Foreman *et al*., 2006). (Lower) Location of the Bering Slope Current and key geographical names in this study. Grey shade denotes the ocean depth.

3. Overview of modeling results

Figure 2 displays a seasonal march of the surface current of the BSC reproduced in the model. The seasonal march of the model well represents variations observed by satellite (Ladd, 2012, 2014). The BSC is the strongest in winter (January to March). It flows over the slope adjacent to the shelf break. The BSC starts separating from the slope, with weakening its strength (April-June). Then, the BSC reaches the deep basin, although the mean current field becomes relatively weak compared with the BSC's amplitude of other seasons. In summer (July-September) the BSC is located at approximately 3 degrees away from the slope. Then, a new BSC starts forming along the slope in fall (October-December).

This seasonal march resembles closely to the BSC's seasonality in reality (Ladd, 2012). The off-slope speed of the BSC axis propagation (depicted by the meridional surface current) along an observation line off the Zhemchug Canyon is approximately 0.013 m s^{-1} from February to July (Fig. 3), consistent with satellite observations (Okkonen, 2001). This off-slope propagation of the BSC is likely associated with the growth of clockwise eddies along the slope during spring to early summer. Figure 4 displays isopycnal depth anomaly from the annual mean on the 27.0 σ_θ, in which we can find anticlockwise eddies' development along the slope. We also find a current reversal in Fig. 3 that develops from April until October, indicating that a stationary eddy forms over the continental slope off the Zhemchug Canyon. Similar eddy development is found off the Pribilof Canyon and Navarin Canyon as well.

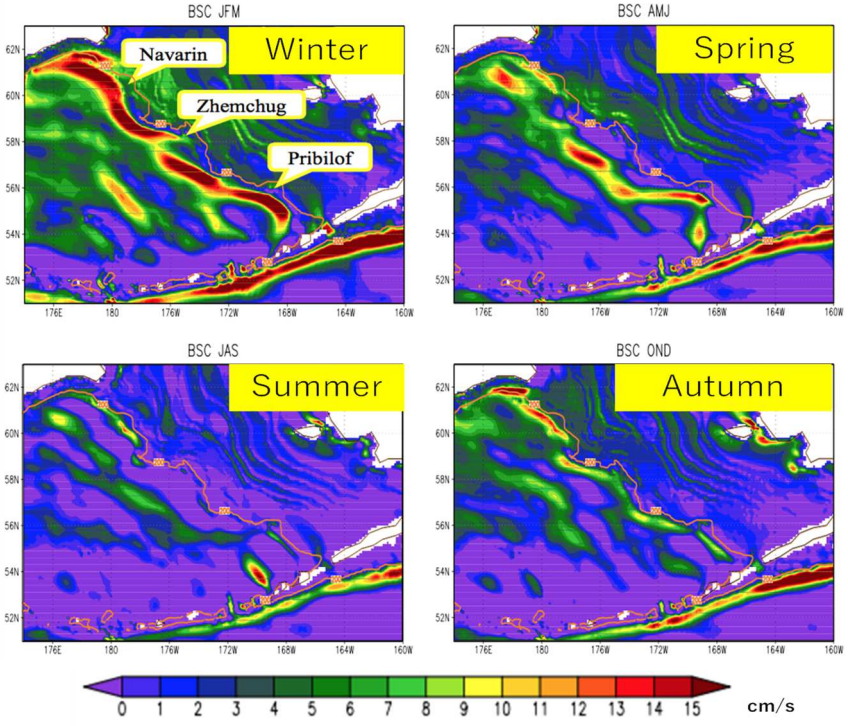

Fig. 2. Seasonal mean of the surface current speed along the shelf break in the Bering Sea. Seasonal evolution of the BSC is shown.

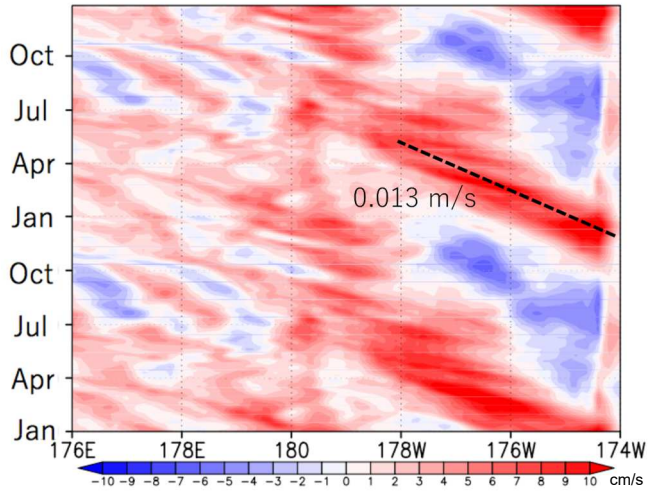

Fig. 3 Hovmöller diagram representing the meridional surface current off the Zhemchug Canyon along 57.5°N. Reddish (bluish) color denotes northward (southward) current (with a unit of cm/s). Dashed line denotes the propagation speed of the BSC axis in the offslope direction.

Figure 4 indicates that during winter, a positive depth anomaly as large as ~40 m is present over the slope confined to the shelf break, while a negative anomaly of ~ -40 m exists off-slope. This corresponds to a steep inclination of the pycnocline, *i.e.* the pycnocline front, where the BSC flows in February. The area of the positive depth anomaly broadens during spring and summer, resulting in the pycnocline deepening away from the slope. The negative anomaly ahead of the positive anomaly propagates westward as well, keeping a steep pycnocline front in-between. On the other hand, a substantial shoaling appears along the shelf break during summer and it broadens westward in fall.

A vertical section of the velocity and density field along 57.5°N reveals that the BSC has a baroclinic jet structure in which the isopycnals of 26.8-27.4 σ_θ incline toward the slope during autumn and winter (Fig. 5). In November, the BSC emerges approximately at 175°W tightly confined to the shelf break with the inclination of the isopycnals toward the slope. The BSC broadens to 176°W in February keeping the baroclinic jet structure. The current is quite deep. It flows northward with a speed as high as 0.03 ms^{-1} at a depth of 1000m, which is consistent with observations by Argo floats (Johnson *et al.*, 2004). Nevertheless, a southward flow can be observed below 600 m immediately adjacent to the slope. In May, the BSC start separating from the shelf break, developing a current reversal in the in-slope side. The BSC moves into the deep basin completely in August. The isopycnals exhibit a bowl shape between 174°W and 179°W, indicating the presence of a stationary anticyclonic eddy. The BSC is recognized as a northward current at 179°W along the limb of the stationary eddy. The BSC's vertical extent is shallower than the BSC in winter.

Anticyclonic eddies with a diameter of 200 km are prominent in a snapshot flow field, consistent with satellite observations (Ladd, 2012). The horizontal scale of eddies is closely related to the scale of the canyons.

As described above, the present model simulates the BSC well. Therefore, the model output was utilized to analyze the seasonality of the BSC and associated eddies.

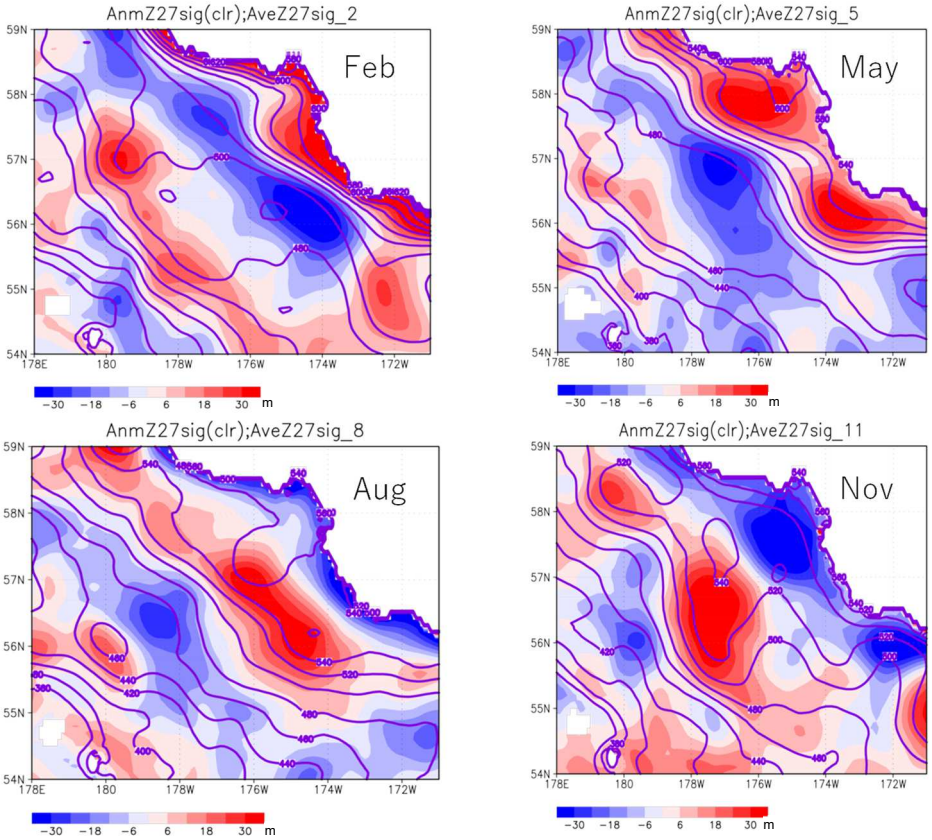

Fig. 4 Color shade depicts sopycnal depth anomaly of 27.0 σ_θ with a unit of m from February to November off the Zhemchug Canyon. Reddish color denotes deepening, while bluish color denotes shoaling. Contours denote depths of the 27.0 σ_θ with the contour interval of 20 m.

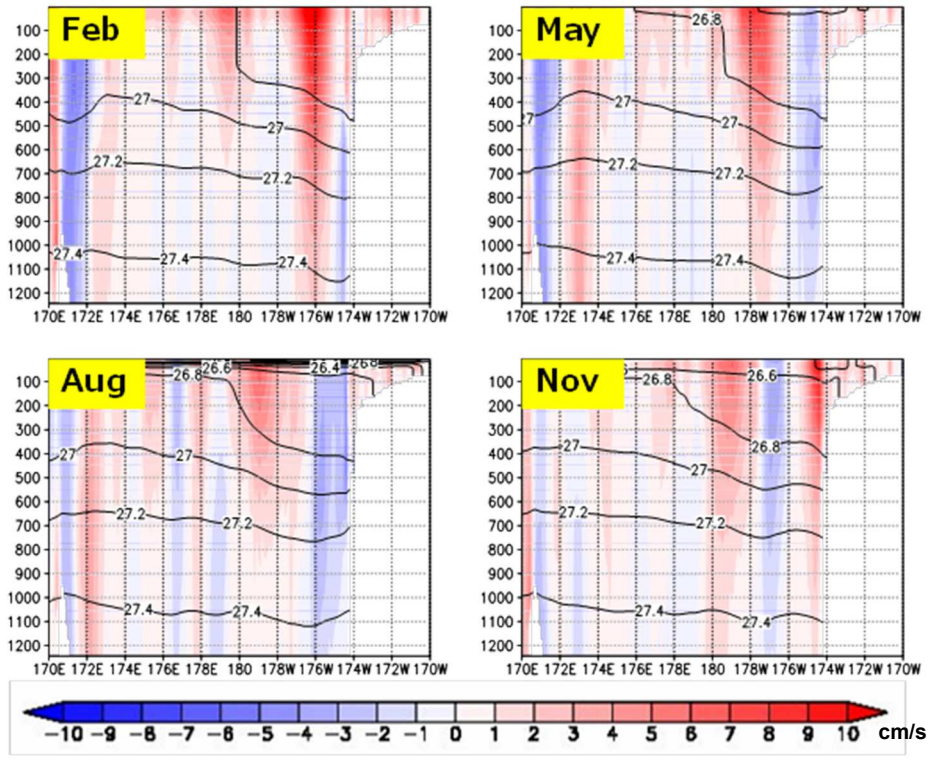

Fig. 5 Vertical sections of meridional current (color shade) and density (contours) on the 57.5°N off the Zhemchug Canyon. Reddish (bluish) color denotes northward (southward) current with a unit of cm/s. Contour interval is 0.2 σ_θ.

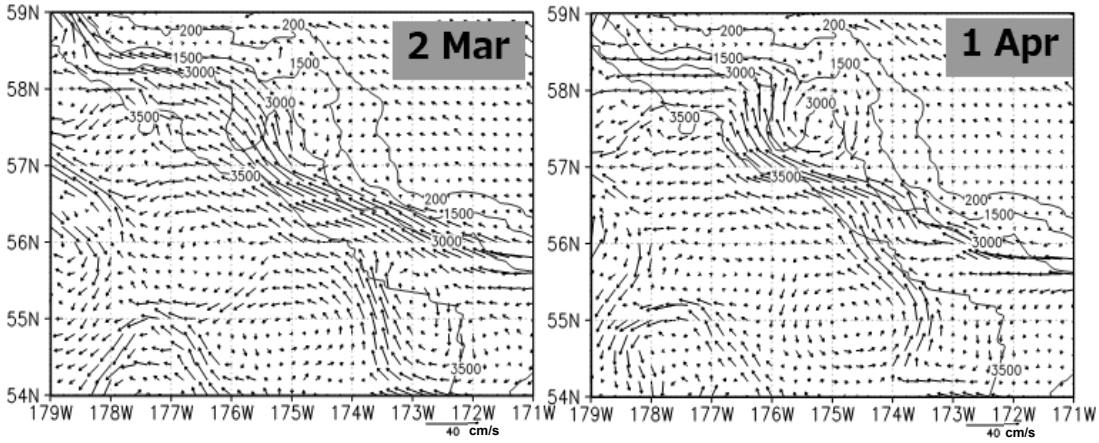

Fig. 6 Evolution of an eddy off the Zhemchug Canyon region. Vector denotes velocity with a unit of cm/s.

4. Eddy generation in shelf-break canyons

We first describe eddy generation processes in the Zhemchug Canyon region (Fig. 6). The BSC flows along the shelf break in mid-February. An anticyclonic eddy starts growing in early March, when the flow is separated from the shelf break in the upstream region of the canyon, because of inertia due to intensification of the BSC. That is, the BSC flows a deep portion of the Zhemchug Canyon. Triggered by this flow separation, the eddy grows to a significant amplitude by early April, and hence, a typical time scale of the eddy growth is of the order of one month. The eddy further grows during spring, thereby pushing the BSC farther off-slope. Since a depth front of 27.0 σθ in mid-March is advected by a barotropic flow, as seen approximately at 57°N, 175°W, the eddy growth and the off-slope movement of the BSC would be caused by baroclinic instability.

Here we examine time scale of the eddy growth in the Zhemchug Canyon seen in Fig. 6 in which a typical time scale of the eddy growth is one month. We use a quasi-geostrophic two-layer model for the upper- and lower-layer stream function ψ_1 and ψ_2, where layer thicknesses are H_1 and H_2, and the along-slope mean flows are U_1 and U_2, respectively. For simplicity, we consider a channel over a β-plane with a typical Coriolis parameter f_0, in which the coastline is rotated by θ from the zonal direction; $\theta \approx -45°$ for the BSC. Then we obtain

$$\left(\frac{\partial}{\partial t} + U_i \frac{\partial}{\partial x}\right) q_i + \frac{dQ_i}{dy}\frac{\partial \psi_i}{\partial x} = 0\,, \qquad (1)$$

where the subscript $i = 1,2$ denotes the upper- and lower-layer variables, and t, x and y denote time, the along-slope and on-slope directions, respectively. q_i and Q_i are perturbed and ambient potential vorticity

$$q_i = \nabla^2 \psi_i - \frac{1}{R_i^2}\left(\psi_i - \psi_j\right),\ i = 1,2,\ j \neq i\,,$$

$$\frac{dQ_i}{dy} = \left(\beta\cos\theta + (-1)^i \frac{U_s}{R_i^2} + \delta_{2i}\frac{f_0 s}{H_2}\right) y,\ \delta_{2i} = \begin{Bmatrix} 0 \text{ for } i = 1 \\ 1 \text{ for } i = 2 \end{Bmatrix},$$

where s denotes a slope, and $U_s = -(U_1 - U_2)$. Note that $U_s > 0$ for the BSC since $U_1 < 0$. R_i is a stratification parameter of each layer

$$R_i^2 = \frac{g' H_i}{f_0^2},$$

where g' is the reduced gravity between the two layers. Here, we assume a gentle slope, *i.e.*, $R_1 s \ll H_1 + H_2$, so that the quasi-geostrophic assumption is valid. This assumption is justified by a fact that the BSC in February flows deep part of the Zhemchug Canyon. Assuming a plane wave solution $\psi_i \propto e^{ik(x-ct)}$, where k is the wave number and c is the eigenvalue of the coupled equation (1), we will obtain a growth rate $k\mathrm{Im}(c)$, where $\mathrm{Im}(c)$ is the imaginary part of the eigenvalue.

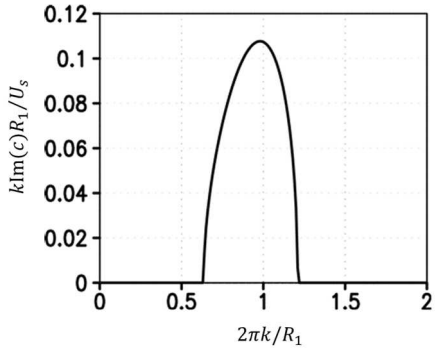

Fig. 7 Scaled growth rate $k\mathrm{Im}(c)U_s/R_1$ vs scaled wavenumber $2\pi R_1/k$.

Figure 7 displays a growth rate for $U_s = 0.05$ ms^{-1}, $H_1 = 800$ m, $H_2 = 2200$ m, $g' = 9.8 \times 7.0 \times 10^{-4}$ ms^{-2}, $f_0 = 1.2 \times 10^{-4}$ s^{-1}, $\beta = 1.2 \times 10^{-11}$ s^{-1}m^{-1} at 57°N. In this case, $R_1 = 1.9 \times 10^4$ m. As for a current with $U_1 = -U_s$ and $U_2 = 0$, then $U_s = 0.05$ms^{-1} gives an observed transport 4.0 Sv of the BSC (*e.g.* Johnson *et al.*, 2004) if a width of 100 km and a depth of 800 m are assumed. Figure 7 indicates that a scaled maximum growth rate is typically 0.1 at a typical (scaled) wavenumber 1.0. Hence, a time scale for the eddy growth $T = [k\mathrm{Im}(c)]^{-1}$becomes $T \approx R_1/(0.1U_s) \approx 44$ days at a wave

length $\lambda \approx 2\pi R_1/1.0 \approx 120$ km. These values are consistent with the simulated results (Fig. 6) as well as satellite observations (Ladd, 2012, 2014). This implies that the eddy growth of the seasonal time scale would be caused by baroclinic instability due to potential energy release associated with the main pycnocline.

To examine the energy source of the eddy growth further, the baroclinic energy conversion rate

$$BC = \frac{g}{\rho_0}\overline{\rho' w'}, \quad \text{(2a)}$$

and the barotropic energy conversion rate

$$BT = -\overline{u'^2}\frac{\partial \bar{u}}{\partial x} - \overline{u'v'}\left(\frac{\partial \bar{v}}{\partial x} + \frac{\partial \bar{u}}{\partial y}\right) - \overline{v'^2}\frac{\partial \bar{v}}{\partial x}, \quad \text{(2b)}$$

(Qiu *et al.*, 2015) were calculated at 200 m. Here, the mean values are defined as the 8-year mean of each month, while the prime denotes deviation from the mean. Since the present simulation is driven by the monthly climatological forcing, the mean values here represent seasonal variations of the BSC and the perturbations represent intra-seasonal variations caused by eddies. The baroclinic energy conversion (equation 2a) occurs along the BSC axis of each month. In February, the region of high conversion rate occurs along the slope where the BSC flows (Fig. 8), consistent with the theoretical results that implies baroclinic instability. The region of the high baroclinic conversion moves off-slope during spring and summer along with the BSC axis propagates off-slope. Intra-seasonal eddies are maintained or even intensified toward summer likely as a result of this continual energy conversion due to baroclinic instability. The barotropic energy conversion rate (equation 2b) is, on the other hand, one order smaller than the baroclinic conversion rate. Therefore, most of EKE stems from the mean potential energy associated with the main pycnocline of the BSC, that is, inclination of the pycnocline toward the slope.

5. Puzzles in the off-slope BSC propagation

What is the mechanism for the westward propagation of the BSC and eddies? We have not succeeded in explaining its mechanism. We first examined whether the westward propagation of annual Rossby waves is possible. The maximum frequency for the baroclinic Rossby wave to exist is

$$\omega_{max} = \frac{1}{2}\beta R_c \quad \text{(3a)}$$

where $R_c = c_g/f_0$ is the Rossby radius of deformation in which c_g is the internal gravity wave phase speed. Annual Rossby waves are present if the angular frequency corresponding to one year Ω_{ann} is smaller than ω_{max}. Equation (3a) condition yields

$$\frac{1}{2}\beta R_c > \Omega_{ann}$$

or

$$R_c > 2\Omega_{ann}/\beta \approx 32.0 \text{ km} \quad \text{(3b)}$$

to be necessary for the existence of Rossby waves. However, the condition (3b) cannot be satisfied in the Bering Sea because $R_c = c_g/f_0$ is evaluated as 16.4 km based on $c_g = 2.0$ ms^{-1} (*e.g.* Killworth *et al.*, 1997), and hence $R_c < 2\Omega_{ann}/\beta$. That is, the existence condition (3b) is not satisfied with respect to the annual period Rossby waves. In conclusion, the annual signal at the shelf break hardly propagates westward as an annual baroclinic Rossby wave train.

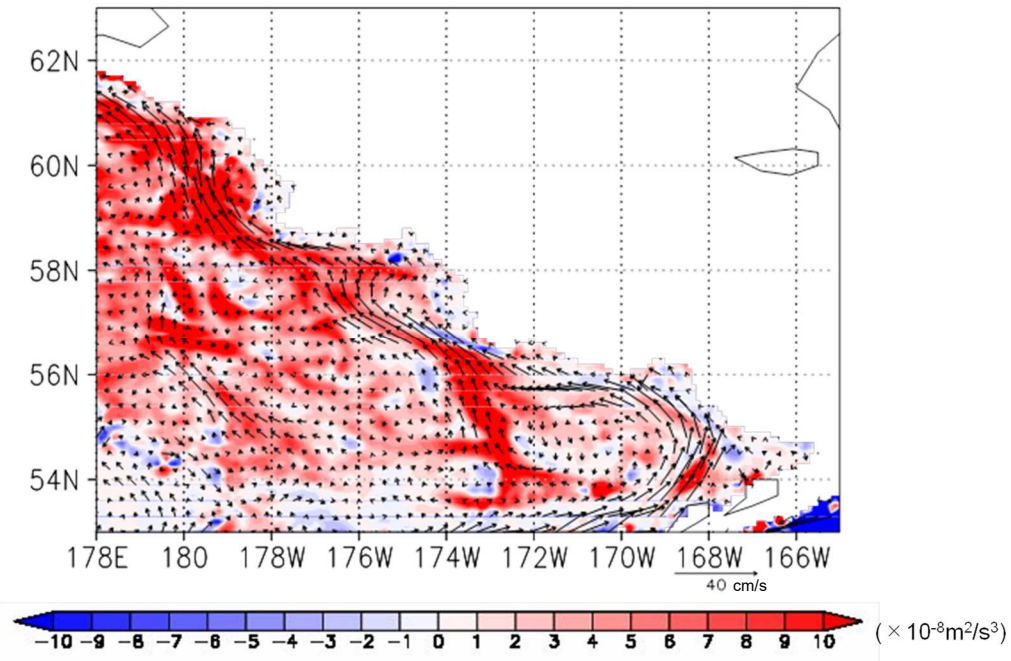

Fig. 8 Color shade depicts the baroclinic energy conversion rate at a depth of 200 m in February along the BSC. Reddish (bluish) color denotes convergence (divergence) of the baroclinic energy. Arrows denote velocity with a unit of cm/s

We also noticed that the propagation of long Rossby waves does not give the answer neither; $c_g = 2.0$ ms^{-1} (*e.g.* Killworth *et al.*, 1997) implies an estimation of the phase speed of the long baroclinic Rossby wave $c_R = -\beta {c_g}^2 {f_0}^{-2}$ to be -0.3×10^{-2} ms^{-1} for $f_0 = 1.2 \times 10^{-4}$ s^{-1}, and $\beta = 1.2 \times 10^{-11}$ s^{-1}m^{-1} at 57°N. The offshore propagation speed in the numerical models is 1.3×10^{-2} ms^{-1} (see Fig. 3), which is faster than the long Rossby waves' estimation. The analyses above suggest that the linear wave theory would not be appropriate for the westward propagation of waves/eddies. Nonlinearity should be taken into account. We are seeking its proper mechanism.

6. Conclusion and discussion

Seasonal variations of the Bering Slope Current (BSC) and eddies were discussed by analyzing an OGCM output. The model output simulates the seasonal variations of the BSC realistically; the BSC flows along the shelf break over the slope in winter, and moves off-slope during spring and summer. Eddies start growing in winter in the shelf-break canyons and cause the BSC's separation from the shelf-break. The eddies obtain kinetic energy converted from potential energy associated with deepening of the main pycnocline of the BSC. The growth rate of the eddies is the order of 1 month. A linear baroclinic instability theory with a sloping bottom can explain this slow growth.

Offslope propagation of the BSC, observed by satellites as well as simulated by the OGCM, is still puzzling. An annual baroclinic Rossby wave is not able to exist because their maximum frequency ω_{max} is smaller than the frequency associated with the annual oscillation. Further, a linear long wave is far slow compared with the propagation speed of the observed and simulated westward propagation. Therefore, the linear theories are not appropriate for the BSC's offslope propagation in the OGCM as well as in reality; nonlinear effects would be important.

The seasonal variation of the BSC is correlated with the deepening of isopycnal levels adjacent to the slope in winter (see Fig. 4). Thus, it is important to understand the mechanism of the wintertime isopycnal deepening to elucidate the BSC's seasonality. One hypothesis is a remote effect of wind forcing in the Gulf of Alaska; the BSC's deepening is apparently correlated with pycnocline deepening along the coast of Gulf of Alaska, which is likely caused by intensified wind stress due to the Aleutian Low. The isopycnal depth anomaly along the shelf break in the Bering Sea can be traced back to the Alaskan Stream via the Aleutian Islands (Fig. 9). Coastally trapped waves may be an agent to link the anomaly between the Gulf of Alaska and the Bering Slope. The study is now underway.

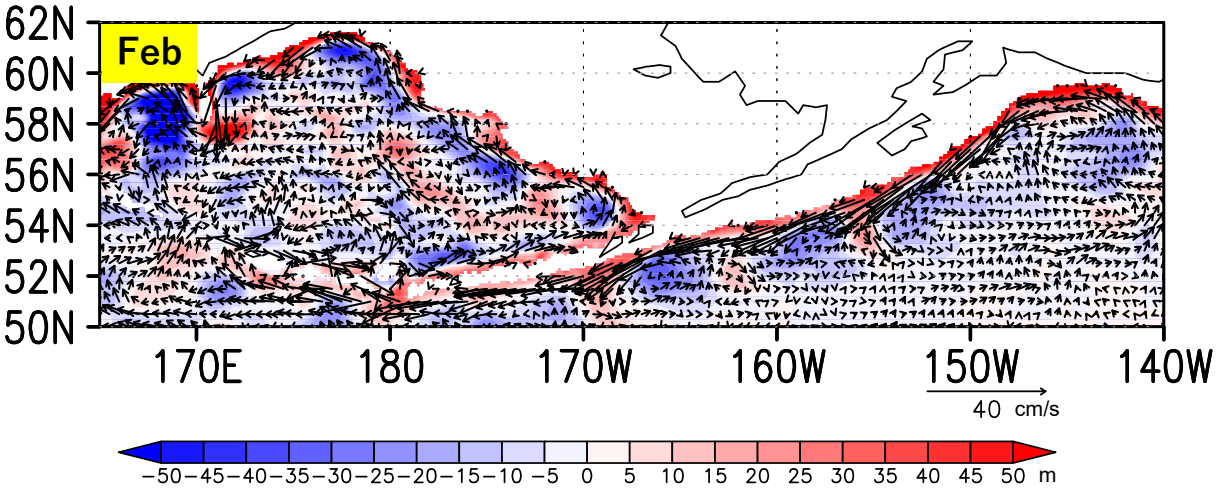

Fig. 9 Isopycnal depth anomaly of 27.0 σ_θ (color shades with a unit of m) in February. Reddish color denotes deepening, while bluish color denotes shoaling. Vectors indicate velocity at 27.0 σ_θ isopycnal surface with a unit of cm/s.

Acknowledgements
This work was supported by KAKENHI (21H01154).

References
Foreman, M.G.G., P. F. Cummins, J. Y. Cherniawsky, and P. Stabeno (2006): Tidal energy in the Bering Sea. *J. Mar. Res.*, **64**, 797-818.

Johnson, G.C., Stabeno, P.J., Riser, S.C. (2004): The Bering Slope Current system revisited. *J.Phys. Oceanogr.*, **34**, 384-398.

Killworth, P.D., D.B. Chelton, and R.A. de Soeke (1997): The speed of observed and theoretical long extratropical planetary waves. *J.Phys. Oceanogr.,* **27**, 1946-1966.

Ladd, C., Stabeno, P.J., O'Hern, J.E. (2012): Observations of a Pribilof eddy. *Deep-Sea Res. I.*,66, 67-76.

Ladd, C. (2014): Seasonal and interannual variability of the Bering Slope Current. *Deep-Sea Res.II.*, **109**, 5-13.

Matsuda, J., H. Mitsudera, T. Nakamura, Y. Sasajima, H. Hasumi, and M. Wakatsuchi. (2015): Overturning circulation that ventilates the intermediate layer of the Sea of Okhotsk and the North Pacific: The role of salinity advection. *J. Geophys. Res.-Oceans.*, **120**, 1462-1489

Mizobata, K. and 8 co-authors (2002): Bering Sea cyclonic and anticyclonic eddies observed during summer 2000 and 2001. *Prog. in Oceanogr.*, **55**, 65–75.

Noh Y, & Jin Kim H. (1999): Simulations of temperature and turbulence structure of the oceanic boundary layer with the improved near‐surface process. *J. Geophys. Res. Oceans*, **104,** 15621-15634.

Okkonen,S.R. (2001): Altimeter observations of the Bering Slope Current eddy field. *J. Geophys. Res*, **106**, 2465-2476

Qiu, B., S. Chen, D.L. Rudnick, and Y. Kashino (2015): A new paradigm for the North Pacific subthermocline low-latitude western boundary current system. *J.Phys. Oceanogr.,* **45**, 2407-2423.

Pickart, R.S., G.W.K. Moore, A.M. Macdonald, I.A. Renfrew, J.E. Walsh, and W.S. Kessler (2009): Seasonal evolution of Aleutian low-pressure systems: Impactions for the North Pacific sub-polar circulation. *J.Phys. Oceanogr.*, **39**, 1316-1339.

Springer, A. M, McRoy, C. P., Flint, M. V (1996): The Bering Sea Green Belt: shelf-edge processes and ecosystem production. Fisheries Oceanography, 5(1996), pp. 205-223.

Tanaka, T., I. Yasuda, K. Kuma, J. Nishioka (2017): Evaluation of the biogeochemical impact of iron-rich shelf water to the Green Belt in the southeastern Bering Sea. *Continental Shelf Res.*, **143**, 130-138.

Summary in Japanese

和文要約

ベーリングスロープカレントの季節変動

三寺史夫[1]、平野洋一[2]、西川はつみ[3]、周宏瑋[4]

[1]北海道大学低温科学研究所, [2]北海道大学環境科学院
[3]東京大学大気海洋研究所, [4]水産研究・教育機構

ベーリングスロープカレント（BSC）の季節変動をモデルのアウトプットを用いて調べた。傾圧不安定によって渦が生じ、それに伴い BSC が大陸棚から離れて沖向きに進んだ。冬季における BSC 表層流の強化が渦形成の原因である。その強化はアラスカンストリームの強化と対応しており、アラスカ湾からの遠隔影響であろうと考えられる。

Correspondence to: H. Mitsudera,
humiom@lowtem.hokudai.ac.jp

Okhotsk Sea and Polar Oceans Research 7 (2023) 30-35

https://doi.org/10.57287/ospor.7.30

Article

Diurnal variation in precipitation and cloud formation during winter in Rikubetsu, inland Hokkaido, northern Japan

Naohiko HIRASAWA[1,2] and Hiroyuki KONISHI[3]

[1] *National Institute of Polar Research, Tachikawa, Tokyo, Japan*
[2] *Department of Polar Science, School of Multidisciplinary Sciences, SOKENDAI (The Graduate University for Advanced Studies), Tachikawa, Tokyo, Japan*
[3] *Division of Math, Sciences, and Information Technology in Education, Osaka-kyoiku University, Osaka, Japan*

(Received November 28, 2022; Revised manuscript accepted January 16, 2023)

Abstract

Rikubetsu (43.5°N, 143.8°E) lies to the east of the central mountain range in Hokkaido, and is separated from the Sea of Japan side where there is a lot of snowfall due to the flow of moist air across this sea. Snowfall in Rikubetsu is primarily associated with synoptic-scale disturbances that move around Hokkaido during the winter season. This study investigated the diurnal variations in precipitation and cloud formation in Rikubetsu in the winters of 2013–2014 and 2014–2015. The results showed that the diurnal precipitation cycle had early morning and afternoon modes throughout the winter of 2013–2014, and a single, early morning mode in the winter of 2014–2015. However, examining only days with low precipitation intensities that were not markedly affected by synoptic-scale disturbances revealed that the early morning and afternoon modes appeared in both winters. The afternoon mode is associated with mountain-valley breezes, with cloud formation beginning in the morning and precipitation occurring in the afternoon. The mechanism for the early morning mode is left for future studies, but it does not involve the development of clear-sky precipitation due to radiative cooling.

Keywords: snowfall, precipitation, cloud, diurnal variation, Rikubetsu

1. Introduction

The accurate measurement of snowfall is affected by factors such as the capture rate of snow particles by instruments, which decreases as the wind speed increases, and the evaporation of captured snowfall before it can be measured. In an attempt to quantitatively clarify and correct for these factors, the World Meteorological Organization (WMO) conducted three international projects titled, "Solid Precipitation Intercomparison Experiment (SPICE)". We participated in the most recent SPICE project using data collected at our observation site in Rikubetsu (Hirasawa *et al.*, 2018) during the winters of 2013–2016 (*e.g.*, Nitu *et al.*, 2018, Qiu, 2012).

Rikubetsu (43.5°N, 143.8°E, 217 m above sea level) is located on the eastern side of the central mountain range in Hokkaido (Fig. 1a). The mountains separate the site from the Sea of Japan side of the island, which typically experiences heavy snowfall during the Asian winter monsoon. The winter monsoon is characterized by cold air being blown from the Eurasian continent toward the Pacific Ocean. The air becomes moist as it crosses the Sea of Japan and causes snowfall on the windward side of mountain ranges as it passes over the Japanese archipelago (*e.g.*, Manabe, 1957). During the heavy snowfall on the Sea of Japan side of Japan during the winter monsoon, most of the areas on the Pacific Ocean side of Japan, including Rikubetsu, generally experience clear skies. Snowfalls in Rikubetsu are mainly due to frontal activity associated with synoptic-scale disturbances passing through the region, which is a common feature of the snowfall/precipitation on the Pacific Ocean side of Japan in winter. As a result, the cumulative precipitation in areas on the Pacific Ocean side of Japan is lower than that on the Sea of Japan side. For example, the amount of cumulative precipitation in Rikubetsu was approximately 150 mm for the period from December 2013 to March 2014 (2013–2014 winter) and 300 mm from December 2014 to March 2015 (2014–2015 winter), while the regions on the Sea of Japan had approximately 1,000 mm of precipitation during the same time period.

Rikubetsu, which is a slightly elevated area that extends from Kitami city in the north to Obihiro city in the south, is one of the coldest areas in Japan (Sorai *et al.*, 2016), with daily winter minimum air temperatures often reaching approximately -30°C. The area is also characterized by clear-sky precipitation (so-called diamond dust) during the coldest hours of the evening (*i.e.*, from midnight to early morning), which occurs due

to radiative cooling. This phenomenon may result in diurnal variation in precipitation, but the underlying mechanisms have not yet been investigated in detail.

Most studies on the diurnal variation in precipitation have been conducted in the warm season or at lower latitudes, such as the in the subtropics (*e.g.*, Watters *et al.*, 2021), and the process of such events is typically discussed in association within the context of land-sea breezes or mountain-valley breezes. Watters *et al.* (2021) emphasized the importance of improving the representation of precipitation amount and frequency in climate models, including in the diurnal cycle.

Oki and Musiake (1994) and Fujibe *et al.* (2006) investigated the diurnal precipitation cycle in Japan. Both groups reported three types of diurnal variation: a single maximum in either the early morning or in the afternoon, and maxima at both times. However, as the analyses of both studies had relatively few observation points in Hokkaido —two in the former study and one in the latter study— their findings are considered to be insufficient for generalizing the features of snowfall in inland Hokkaido. Nonetheless, their results are helpful for this study. Noh *et al.* (2004) reported a diurnal cycle in snowfall around Wakasa Bay, on the Sea of Japan side of Honshu, the main island of Japan. Maximum snowfall was observed over the land during the daytime and over the ocean at night in association with localized land-sea breezes.

In order to better understand the climate of cold regions, it is important to estimate the quantitative contribution and mechanisms of diurnal variation in precipitation and moisture circulation. However, our knowledge of the current situation in Hokkaido in winter is lacking. This study therefore investigated the diurnal variation in precipitation and cloud formation in Rikubetsu in the winters of 2013–2014 and 2014–2015 which were treated as being representative of inland conditions on the Pacific Ocean side of Hokkaido.

2. Observations

We have been conducting snowfall and meteorological measurements at the observation site in Rikubetsu since 2012 (Fig. 1b). The data used in this study were collected using a ceilometer (CT25K, Vaisala, Finland; Fig. 1c), a snowfall weighing gauge (T-200B, Geonor, Norway; Fig. 1d) (referred to as Geonor), a disdrometer (Laser Precipitation Monitor (LPM), Theis, germany; Fig. 1e), and a meteorological sensor (WXT530, Vaisala). The Geonor measurements provided the reference data for the SPICE project.

The ceilometer recorded the cloud-base height and vertical profile of backscatter intensity every 15 s. The LPM recorded the precipitation intensity derived from laser attenuation measured every 1 min. The Geonor recorded the precipitation intensity based on changes in the weight of captured and cumulative precipitation in the gauge every 1 min. Understanding the differences in measured snowfall intensities between various instruments was one of the aims of the SPICE; however, such comparisons were beyond the scope of this study, which used the Geonor to check the measurements by the LPM. The main instrument used to measure precipitation in this study was the LPM because most snowfall in Rikubetsu was light, and the LPM detected light snowfall better than the Geonor.

The WXT530 meteorological sensor was used to measure pressure, temperature, relative humidity, wind speed, and wind direction every 15 s. The wind sensor was of the ultrasonic type. Since the temperature and humidity sensors employ natural ventilation, the temperature may have been overestimated when insolation was high and wind speeds were low. However, these factors were not considered to be problematic in this analysis because we did not perform quantitative evaluations, such as heat balance calculations.

The observation periods were December 1, 2013–March 31, 2014 and December 1, 2014–March 31, 2015, with a start date of December 15, 2013 for the meteorological observations.

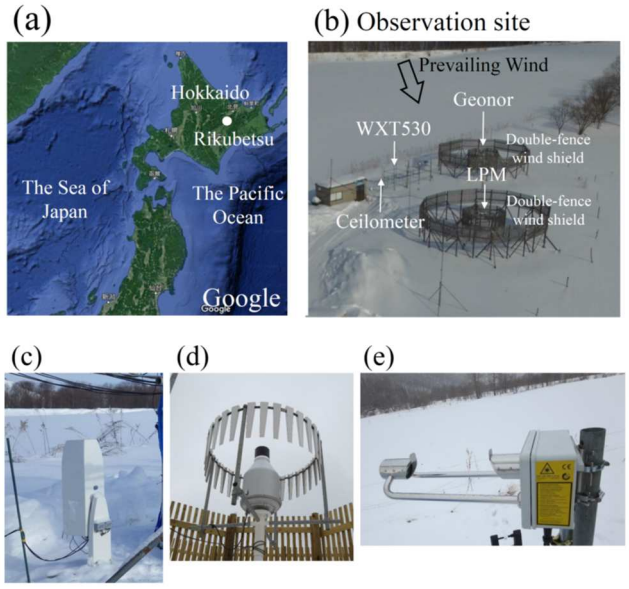

Fig. 1 (a) Map of Hokkaido showing Rikubetsu and topography of region. (b) Landscape surrounding observation site. (c) Ceilometer. (d) Geonor within double-fence windshield. (e) Disdrometer.

3. Precipitation and cloud formation

3.1 Precipitation amount

Figure 2 shows the time series of precipitation intensity and cumulaive precipitation for the two winters. The cumulative precipitation increased step-wise at higher precipitation intensities, mainly due to synoptic-scale disturbances around Hokkaido. The cumulative precipitation measured by the LPM and the Geonor

differed slightly. Nonetheless, the timing and magnitude of the step-wise increases were consistent with each other, except for an event on December 17, 2014.

The total snowfall measured by the LPM in the 2014–2015 winter was 384.4 mm, nearly twice the value of 221.5 mm for 2013–2014. The 2014–2015 winter had more frequent and larger precipitation events than those in 2013–2014.

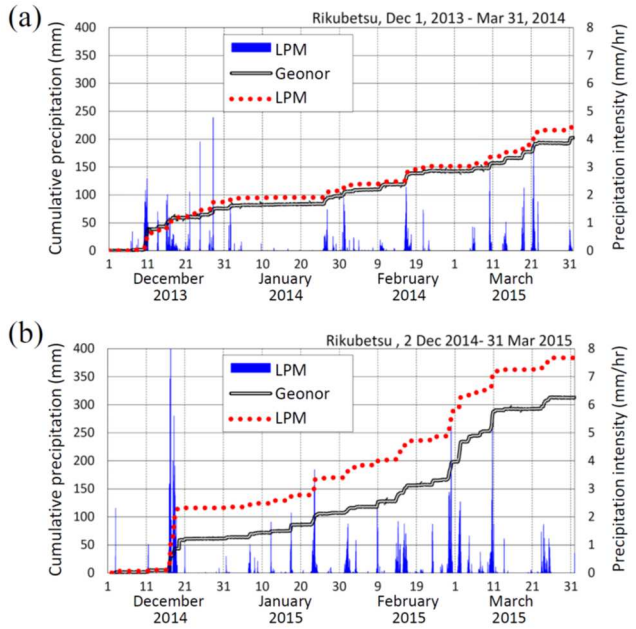

Fig. 2 Time series of cumulative snowfall (mm water equivalent (w.e.)) measured by LPM, Geonor, and precipitation intensity (mm/hr w.e.) measured by LPM (a) for 2013–2014 winter and (b) for 2014–2015 winter.

3.2 Diurnal variation in precipitation

Figure 3a shows the diurnal changes in hourly cumulative precipitation for each of the two winters: while the winter of 2013–2014 had a bimodal variability with local maxima in the early morning and afternoon, the winter of 2014–2015 had a broad peak from 22:00 to 8:00 with a local maximum from 7:00 to 8:00.

The analyses by Oki and Musiake (1994) and Fujibe *et al.* (2006) show that the early morning and afternoon modes tend to appear in the diurnal cycle of precipitation in Japan. In this analysis of the two winters, the early-morning mode was observed frequently in both winters, while the afternoon mode appeared only in the 2013–2014 winter.

Although the passage of synoptic-scale disturbances, which is the main cause of precipitation in Rikubetsu, should be independent of the diurnal precipitation cycle, the findings suggest that the atmospheric circulation associated with synoptic-scale disturbances may be influenced by the diurnal cycle.

Next, we examined the diurnal cycle of precipitation events that were not related to synoptic-scale disturbances, including relatively intense precipitation of 0.5 mm/hr or more. Therefore, days with weak precipitation intensity (minor precipitation days) were selected based on the following two criteria: 1) precipitation did not exceed 0.5 mm/hr on that day; 2) precipitation on that day was not an extension of a precipitation event of 0.5 mm/hr or more that started on the preceding day, or that extended to the following day. Minor precipitation days numbered 36 days in the winter of 2013–2014 and 30 days in the winter of 2014–2015. The total precipitation attributed to these minor precipitation was 10.7 mm (4.8% of the winter total) and 5.3 mm (1.4%), respectively.

Figure 3b shows the diurnal cycle in hourly cumulative precipitation for these minor precipitation days. Both winters had a bimodal variation pattern, with early morning and afternoon modes. The results suggested that afternoon precipitation is stronger than early morning precipitation when synoptic-scale disturbance effects are relatively weak and diurnal forcing is more strongly in effect.

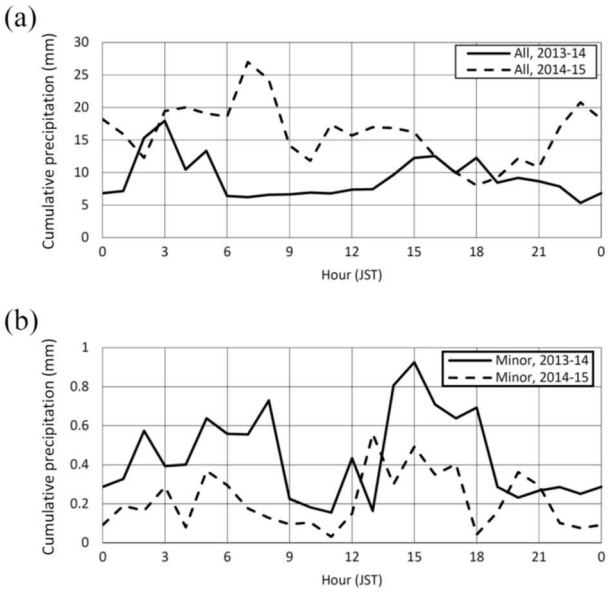

Fig. 3 Diurnal cycle of hourly cumulative precipitation (mm) during winter, (a) for all days in 2013–2014 and 2014–2015 winters, and (b) for days with minor precipitation in 2013–2014 and 2014–2015 winters.

3.3 Diurnal variation in cloud formation

Figure 4 shows the diurnal cycle of clouds in the lower troposphere (<3000 m elevation) as detected by the ceilometer. The vertical axis is the number of days when clouds were detected at that time during the study period; *i.e.*, data for all 121 days from December to March are shown in Fig. 4a, and data for all 36 (30) days with minor precipitation during the 2013–2014 (2014–2015) winter are shown in Fig. 4b.

For all days in the 2013–2014 winter (Fig. 4a), the number of days with clouds increased from 9:00 to 10:00

(JST) and decreased from 17:00 to 18:00. There were 60 to 70 days when cloud formation occurred during the daytime, and 40 to 50 days when cloud formation occurred at night. The number of days with clouds during the daytime was about 1.5 times that at night. On the other hand, in the 2014–2015 winter, a small-amplitude diurnal cycle appeared with more frequent (approximately 60 or 50 days) cloud formation from midnight to early morning from late morning to evening.

The main features in Fig. 4b are the same as those in Fig. 4a. In the 2013–2014 winter, the afternoon mode was more pronounced for the minor precipitation days (25 days, 69%) than for all days (72 days, 60%). In the winter of 2014–2015, although an afternoon mode did not appear for minor precipitation days, there was a relative increase in the ratio of minor precipitation days (21 days, 70%) in the afternoon compared to all days (58 days, 48%), which may be related to the afternoon mode of precipitation.

The difference between the two winters in the diurnal cycle of cloud frequency may be due to differences in the frequency of synoptic-scale disturbance effects, but further study is needed.

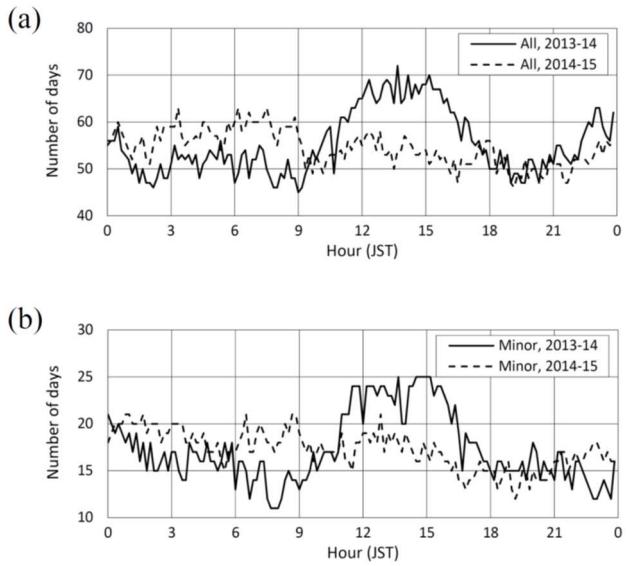

Fig. 4 Diurnal cycle of clouds in lower troposphere (*i.e.*, <3000 m elevation) as detected every 10 min by ceilometer, (a) for all days in 2013–2014 and 2014–2015 winters, and (b) for minor precipitation days in 2013–2014 (36 days) and 2014–2015 (30 days) winters.

4. Discussion

4.1 Afternoon mode

Figure 5 shows a time-altitude section of the backscatter coefficients observed using the ceilometer (Fig. 5a) and the time series of cumulative precipitation observed by the LPM (Fig. 5b) on February 7, 2014, which was one of the minor precipitation days. The ceilometer was used to continually observe clouds with relatively intense backscatter coefficients from 10:00 to 21:00 at altitudes below 3000 m. Touchdowns of the ceilometer signals with the ground indicate precipitation. The LPM detected precipitation from 15:00 to 18:00, but no precipitation was detected at 12:00 and 13:00, when the backscatter coefficients were relatively weak. On the other hand, no precipitation was detected by the LPM when relatively strong backscatter was detected around 20:00; however, it is possible that this was associated with fog. In this case, cloud formation began around 10:00, with relatively strong precipitation observed after 15:00. These features are representative of the daytime mode of cloud formation seen during the 2013–2014 winter season (Fig. 4a) and the afternoon mode of precipitation (Fig. 3b).

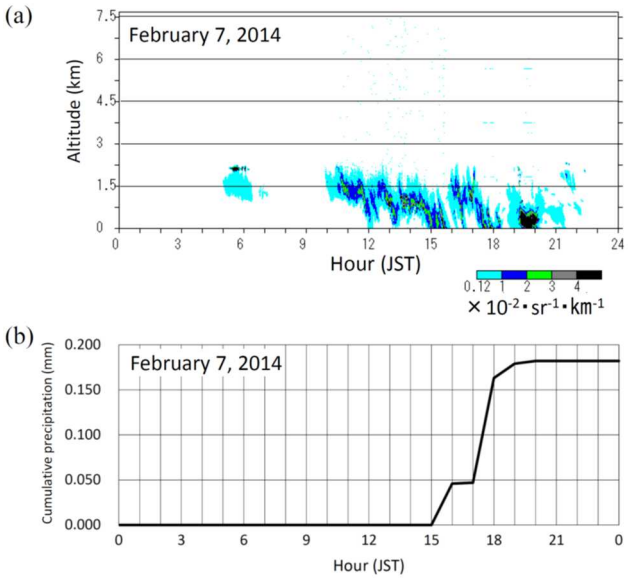

Fig. 5 Daily time series of clouds and precipitation on February 7, 2014. (a) Time-altitude section of backscatter coefficients determined by ceilometer. The color bar shows the magnitude of the backscatter coefficients. (b) Time series of hourly cumulative precipitation observed by LPM.

Figure 6 shows hourly changes in air temperature, relative humidity to ice (Fig. 6a), wind speed (WS), and wind direction (WD) (Fig. 6b) on February 7, 2014.

At approximately 7:00, when the temperature began to rise, the wind speed decreased, and the wind direction became less constant from the west at night. At approximately 10:00, when clouds began to form, the wind speed increased and the wind direction became constant to the south-southwest. The daily variation of this wind system represents the mountain-valley breeze cycle. Further, the formation of clouds during the daytime and precipitation in the afternoon can be attributed to the diurnal cycle in this wind system. On the

other hand, the wind direction is from the Pacific Ocean, but the wind speed is weak, which means that the air over the sea will not reach Rikubetsu during the diurnal cycle alone.

By the time the relatively strong precipitation occurred, the wind speed had weakened again, and the wind direction was not constant. It is considered likely that the wind was no longer forced upslope at this time of day. The increase in the relative humidity from 15:00 to 18:00 can be attributed to evaporation (sublimation) of precipitation particles.

In the event that the precipitation particles evaporate (sublimate) completely as they fall from the cloud base, no precipitation would be observed on the ground while clouds were forming. Such a case was observed on January 17, 2013, as shown in Fig. 7, which shows a time-altitude section of the backscatter coefficients determined by the ceilometer. The ceilometer continually observed clouds with relatively intense backscatter coefficients at an altitude of approximately 1500 m from 11:00 to 16:00, with no touchdowns of the signals on the ground. In this case, no snowfall was detected by the LPM or the Geonor.

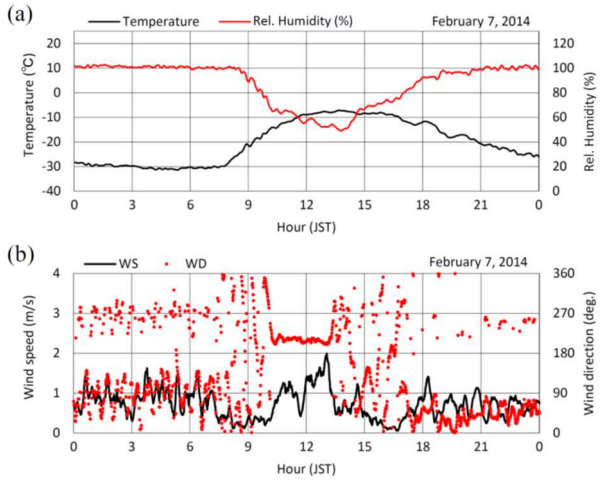

Fig. 6 Daily time series of (a) air temperature, relative humidity to ice, and (b) wind speed and direction on February 7, 2014. The data interval is 1 min, but the wind direction is a 10-min moving average.

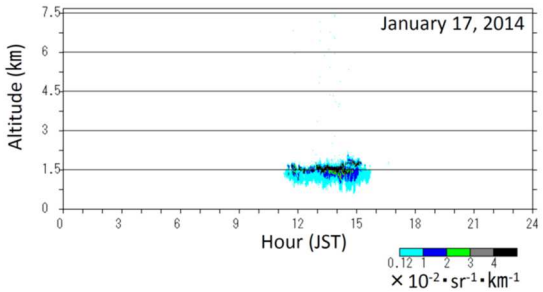

Fig. 7 Same as Fig. 5a, but for January 17, 2014.

4.2 Early morning mode

Figure 8 shows the time series of the cumulative precipitation amount (mm) measured by the LPM during 5:00–8:00 on the minor precipitation days. Twelve of the 36 minor precipitation days had early morning (5:00-8:00) precipitation. The precipitation amount during this period was less than 1 mm on almost all days.

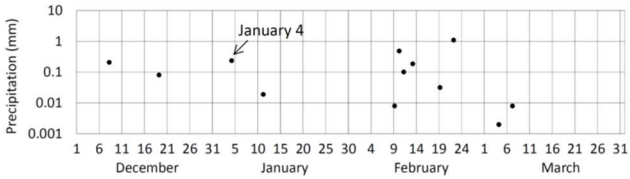

Fig. 8 Time series of cumulative precipitation (mm) measured by LPM during 5:00-8:00 on minor precipitation days. Subsequent figures show the data observed on January 4, 2014.

Figure 9 shows a time-altitude section of the backscatter coefficients determined by the ceilometer (Fig. 9a) and the time series of cumulative precipitation observed by the LPM (Fig. 9b) on January 4, 2014, which is one of the minor precipitation days. The ceilometer observed touchdowns with relatively intense backscatter coefficients below 3000 m from 5:00–12:00, and relatively weak ones from 15:00–20:00. Precipitation was detected by the LPM during the former time period.

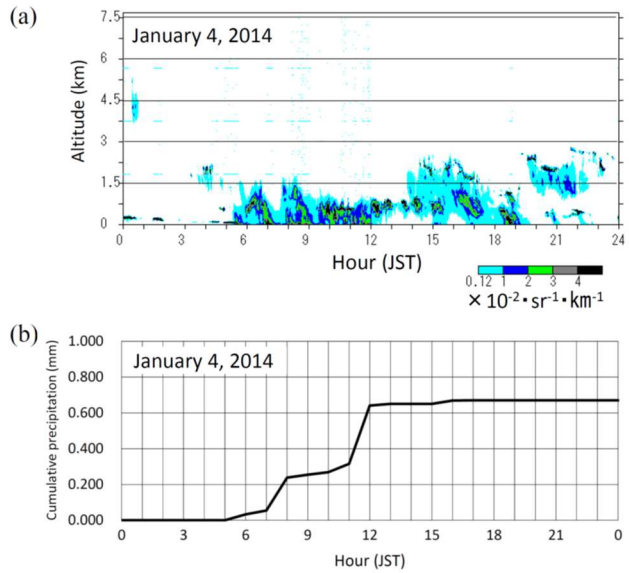

Fig. 9 Same as Fig. 5, but for January 4, 2013.

Figure 10 shows the daily time series of air temperature and relative humidity to ice on January 4, 2014. Temperatures reached their lowest point at around 5:00 when precipitation began. Since this was before sunrise, the increase in temperature after 5:00 is considered to be due to the suppression of radiative cooling by the increase in downward longwave radiation

caused by cloud formation. The relative humidity was typically maintained at 100% when there was no precipitation during the night (see Fig. 6a), but on this morning, the relative humidity fell below 100% with the onset of precipitation. In all other cases of early morning precipitation, the relative humidity was also below 100% during the precipitation period, implying that the early morning precipitation observed in this study is not clear-sky precipitation.

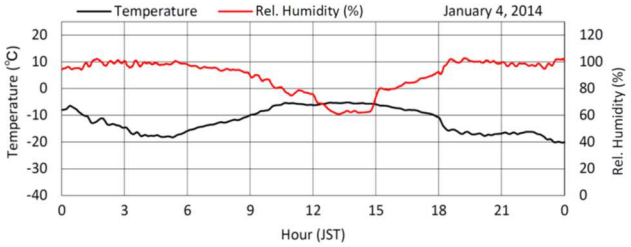

Fig. 10 Same as Fig. 6a, but for January 4, 2013.

5. Conclusion

Rikubetsu is located on the eastern side of the central mountain range in Hokkaido, which separates the site from the Sea of Japan side of the island. Snowfall in Rikubetsu is mainly brought about by synoptic-scale disturbances around Hokkaido that occur several times during the winter season from December to March. This study investigated the diurnal variation in precipitation and cloud formation in Rikubetsu in the winters of 2013–2014 and 2014–2015. The total precipitation in the 2014–2015 winter was nearly twice that in the 2013–2014 winter, implying that the influence of synoptic-scale disturbances was greater in the 2014–2015 winter.

The results showed that the diurnal cycle of precipitation had early morning and afternoon modes throughout the 2013–2014 winter, but only a single mode in the early morning in the 2014–2015 winter. Examining only the days of weak precipitation intensity (minor precipitation days), which are not considered to be strongly influenced by synoptic-scale disturbances, the early morning and afternoon modes appeared in both winters. The afternoon mode is associated with mountain-valley breezes, with cloud formation beginning in the morning and precipitation occurring in the afternoon. On the other hand, the mechanism underlying the early morning mode is left for future studies, but it is not attributed to the formation of clear-sky precipitation due to radiative cooling.

References

Fujibe, F., Yamazaki, N., and Kobayashi, K. (2006): Long-Term Changes in the Diurnal Precipitation Cycles in Japan for 106 Years (1898-2003). *J. Meteorol. Soc. Japan*, **84**(2), 311–317. https://doi.org/10.2151/jmsj.84.311

Hirasawa, N., H. Konishi, K. Nishimura, C. Genthon and project group of Japan Meteorological Agency (2018): SPICE site report: Rikubetsu, Japan. WMO Solid Precipitation Intercomparison Experiment (SPICE), *Instruments and Observing Methods*, **131**, Annex 8.3, December 2018.

Nitu, R., and 42 co-authors (2018): WMO Solid Precipitation Intercomparison Experiment (SPICE). *Instruments and Observing Methods*, **131**. https://library.wmo.int/opac/

Noh, Y.-J., Liu, G., Balas, N., Aonashi, K., and Koike, T. (2004): Diurnal variations of snow precipitation in Wakasa Bay during winter. *J. Meteor. Soc. Jpn.* Ser. II, **82**, 1117–1128. https://doi.org/10.2151/jmsj.2004.1117

Oki and Musiake (1994): Seasonal Change of the Diurnal Cycle of Precipitation over Japan and Malaysia. *Journal of Applied Meteorology and Climatology*, **33**(12), 1445–1463.

Qiu, J. (2012), Snow survey hopes for avalanche of data, *Nature*, **491**, 312-313. https://doi.org/10.1038/491312a

Sorai, T., H. Hamada, T. Kameda, and S. Takahashi (2016): Rikubetsu, the coldest town in Japan: according to the meteorological data by Japan Meteorological Agency from 2007 to 2016 in winter seasons. *Tenki*, **63**, 879-887. (in Japanese)

Watters, D., Battaglia, A., and Allan, R. P. (2021): The diurnal cycle of precipitation according to multiple decades of global satellite observations, three CMIP6 models, and the ECMWF reanalysis. *J. Climate*, **34**, 5063–5080. https://doi.org/10.1175/JCLI-D-20-0966.1

Yamashita, K., S. Nakai, and H. Motoyoshi (2018): Measurements at Joetsu (Japan) for the WMO/CIMO SPICE Project. WMO Solid Precipitation Intercomparison Experiment (SPICE), *Instruments and Observing Methods*, **131**, Annex 8.4, December 2018.

Summary in Japanese

和文要約

北海道内陸部陸別町における冬季の降水量と雲形成の日変化

平沢尚彦 [1,2], 小西啓之 [3]

[1] 国立極地研究所, [2] 総合研究大学院大学, [3] 大阪教育大学

陸別（北緯 43.5 度，東経 143.8 度，標高 217m）は，北海道の中央山脈の東側に位置し，日本海を渡る湿潤な気流により降雪量の多い日本海側とは隔てられている．陸別の降雪は主に北海道付近を通過する総観規模擾乱によってもたらされ，冬季に数回発生する．本研究では 2013-14 年と 2014-15 年の 2 冬における陸別の降水量と雲形成の日変化を調査した．その結果，降水量の日変化には，2013-14 年冬には早朝と午後に極大があり，2014-15 年冬には早朝に極大があることが分かった．また，総観規模擾乱の影響を強く受けていないと考えられる降水強度の弱い日だけを調べると，両冬とも早朝と午後に極大が現れた．午後の極大は山谷風と関連しており，午前中に雲形成が始まり，主に午後に降水が発生する．早朝の極大は放射冷却に伴う晴天降水ではないことが示され、その仕組みの解明は今後の研究に残した．

Correspondence to: N. Hirasawa, hira.n@nipr.ac.jp

ISSN 2436-1550
Online ISSN 2436-2034

Submission Information for OSPOR

Reviewing processes of OSPOR

1) When manuscripts have been received by the Editor-in-Chief, an acknowledgement of receipt will be sent to the author(s) by e-mail. The Editor-in-Chief chooses an editor to handle the manuscript review.
2) The submitted manuscript will be subjected to screening review for its scope, novelty, completeness, English level, and conformation to the OSPOR policy. A manuscript not passing the screening review will immediately be returned to the authors.
3) The editor in charge will select expert reviewers to evaluate the manuscript.
4) As to results of review, if the editor decides that the paper needs revision by the author(s), the manuscript will be returned to the author(s) for revision.
5) Manuscripts returned to author(s) for revision should be resubmitted promptly. If the revision cannot be finished within a month, the manuscript will be regarded as having been withdrawn.
6) The Editor-in-Chief will finally decide whether to accept the manuscript for publication.

Paper Submission

Submission Guideline

All manuscripts should be submitted in digital format (PDF or WORD) with the OSPOR submission sheets (PDF or WORD, offered from OSPOR) by email to the OSPOR Editorial Board

OSPOR Editorial Board

Polar Oceans Research Association (OSPORA)
Address: Kaiyo Koryukan, 1 Kaiyo Koen, Mombetsu, Hokkaido 094-0031 Japan
E-mail: momsys@okhotsk-mombetsu.jp
Phone: +81-158-26-2810 (0158-26-2810 in Japan)
Fax: +81-158-26-2812 (0158-26-2812 in Japan)

Publication Charge

Authors of their institutions are requested to pay the publication charge according to the following rate when paper is accepted. The maximum pages are 6 pages.

1,500 Yen / page within the maximum pages
3,000 Yen / page over the maximum pages (Excess charge)

Copyright

Copyright for an article submitted to OSPOR is transferred to OSPORA when the article is published in OSPOR in any form.

Preparation of manuscripts

The manuscript should be formatted in the form of OSPOR template offered from the OSPORA office, which satisfies the following requirements. The maximum pages in printing style are **6 pages**. Otherwise, an overage fee will be charged.

1) Text
   a) The manuscript should be in the international size A4 in camera-ready style according to the form of OSPOR template.
   b) The first page should include: the title, the author(s) name(s) and their affiliations. If possible, a Japanese translation of the title and the name(s) of the author(s) should be provided in the end of manuscript. If they are not, the translation will be undertaken by the OSPOR editorial board.
   c) An abstract not exceeding 250 words must be provided.
   d) Up to five keywords that describe the content for indexing purposes must be provided.

2) References

a) A list of cited references should be arranged alphabetically. Journal abbreviations are better to use, but when the abbreviation is not known, the full title of the journal should be used in the list.

In the case of many authors, the author name can be written in short as below.

Kawamura, K., F. Parennin and 16 co-authors (2007): Northern hemisphere forcing of climatic cycles in Antarctica over the past 360,000 years. *Nature*, **448**, 912-916.

b) References in the text will include the name(s) of the author(s), followed by the year of publication in parentheses, *e.g.* (Clark, 2003), (Li and Sturm, 2002), (Harrison *et al.*, 2001).

3) Units

Numerical units should conform to the International System (SI).
Units should be in the form as kg m^{-3} not as kg/m^3.

4) Tables

A title and a short explanation should be located on the top of table.
They should be referred to in the text.

5) Figures

a) All Figures (illustrations and photographs) should be numbered consecutively.
b) All Figures should be of good quality and referred to in the text.
c) Figure captions should be located on the bottom of the Figures.

6) More information

For more information about manuscript instruction, please ask to OSPORA office or see OSPORA home page in http://okhotsk-mombetsu.jp/okhsympo/top-index.html

Recent information

Resent information can be get from the following URL.

General Information: http://okhotsk-mombetsu.jp/okhsympo/artical-J/Info-artical.html
Instruction: http://okhotsk-mombetsu.jp/okhsympo/artical-J/Instruction-J.html
Template: http://okhotsk-mombetsu.jp/okhsympo/artical-J/Template-J.html
Submission Sheet: http://okhotsk-mombetsu.jp/okhsympo/artical-J/submiss-sheetJ.html

Organized and sponsored by

City of Mombetsu
Arctic Research Center, Hokkaido University (ARC)

Okhotsk Sea and Polar Oceans Research, Vol. 7 (2023, February)

Published by the Okhotsk Sea and Polar Oceans Research Association (OSPORA),
Mombetsu City, Hokkaido, Japan

Executive Committee of OSPORA:
Chairman: Shuhei Takahashi (Okhotsk Sea Ice Museum of Hokkaido, Director)
Secretariat: Eriko Uematsu
Address: Kaiyo Koryukan, 1 Kaiyo Koen, Mombetsu, Hokkaido 094-0031 Japan
E-mail: momsys@okhotsk-mombetsu.jp
Phone : +81-158-26-2810 (Japan 0158-26-2810)
Fax: +81-158-26-2812 (Japan 0158-26-2812)
http://okhotsk-mombetsu.jp/okhsympo/top-index.html

Okhotsk Sea and Polar Oceans Research

Published by the Okhotsk Sea and Polar Oceans Research Association (OSPORA)
Mombetsu City, Hokkaido, Japan

Vol. 7